International Journal of Disaster Risk Reduction 142 (2026) 106072

Contents lists available at ScienceDirect

International Journal of Disaster Risk Reduction

journal homepage: www.elsevier.com/locate/ijdrr

A novel dynamic disaster risk assessment of Urban Built Environments: An application to flood and earthquake

Enrico Quagliarini [a], Alessia Freddo [b], Caterina Alighieri [a], Maud Natalucci [a], Gabriele Bernardini [a,*]

[a] DICEA Department, Università Politecnica delle Marche, Ancona, Italy
[b] DICAR Department, Università di Catania, Catania, Italy

ARTICLE INFO

Keywords:
Risk assessment
Flood risk
Earthquake risk
Urban built environment
Urban open spaces
User exposure
User vulnerability

ABSTRACT

Disaster risk assessment in Urban Built Environments (UBEs) must consider the joint impacts of possible hazard conditions and dynamics in UBE use, and thus the spatiotemporal variations in the number (exposure) and typology (individual vulnerability) of the hosted population. The integration of such concepts could be boosted by multiscale approaches representing the complex interactions among the UBE subsystems, supporting scenario creation. Building-level data should be aggregated at the scale of urban public open spaces (e.g., streets, urban squares), due to their relevance for user UBE use in normal and emergency conditions. This work adopts this open-space-centred approach and defines a novel methodology for dynamic single-risk assessment in UBEs, combining physical vulnerability, hazard, user exposure and vulnerability. The methodology is applied to flood and earthquake risks, as relevant disasters for UBEs, and allows to mark relevant "hot-spots" in UBE, in these two relevant disasters, and considering different spatio-temporal dynamics in user factors. Validated methods for building-scale analysis of risk factors are adapted to calculate risk assessment indexes at the open space level, including alternative scenarios of hazard (in terms of flood/earthquake severity) and typical occupancy schedules in UBE use. The application to a relevant UBE demonstrates the approach capabilities in detecting open spaces which represent recurrent and scenario-sensitive "hot-spots" to floods and earthquakes, and remarks how consistent risk-level differences exist due to the use dynamics. The proposed method can support decision-makers in intervention prioritisation, focusing on common "hot-spots", and tailoring risk-mitigation and management strategies, depending on the specific scenario.

1. Introduction

Performing disaster risk assessment tasks in Urban Built Environments (UBEs) implies understanding which scenarios can be generated by the combination of several factors related to cities and their communities, as well as to the complex multi-interactions among them [1–4]. It hence represents one of the pillars within the disaster risk management cycle, mainly comprising activities referred to the preparedness stage [5,6]. In fact, as also remarked by the Sendai Framework for Disaster Risk Reduction (Priority 4) [7], preparedness-oriented risk assessment aims to anticipate the potential consequences of hazardous events before they occur, moving

* Corresponding author.
E-mail address: g.bernardini@staff.univpm.it (G. Bernardini).

https://doi.org/10.1016/j.ijdrr.2026.106072
Received 2 September 2025; Received in revised form 3 January 2026; Accepted 21 February 2026
Available online 24 February 2026

towards a more effective response and towards "Build Back Better" (BBB) in recovery, rehabilitation, and reconstruction, exploring plausible scenarios that combine components about hazard, vulnerability and exposure. This perspective is particularly relevant for Sudden Onset Disasters (SUODs), such as earthquakes, floods, urban and wildfires, terrorist acts, volcanic events, tsunamis, cyclones and landslides [8–11]. SUODs can rapidly emerge in the UBE, potentially causing significant damage to the population, buildings, and infrastructures, while simultaneously requiring the activation of emergency procedures and immediate response. These effects depend on the specific characteristics of parameters about hazard, physical vulnerability of UBE placed in SUOD-prone areas, and user factors (including their exposure, individual vulnerability and behaviours) and on how they are combined in a given emergency scenario [12–16].

Considering the different SUODs, the importance of such issues is mainly relevant considering floods and earthquakes, in view of their massive and widespread effects on UBEs. These effects, in fact, are exacerbated by rapid and growing urbanisation phenomena, as also demonstrated by statistics on the impact and damage levels on the urban communities [16–20]. Moreover, these data underline how the severity of such disasters also depends on the spatiotemporal variables, which are strictly connected to the dynamics in the use of the UBE by the population [14,21–24]. Cities as attractor poles in the surrounding territories and touristic cities own additional complexities due to the spatiotemporal variability in the number, position and typologies of users, considering both residents and non-residents [25,26].

Therefore, scenario creation and, thus, risk assessment tasks in these UBEs have to include the analysis of variations about daily commuting, touristification, and seasonal fruition conditions, along with the definition of possible event conditions due to the combination between hazard and physical vulnerability [27,28]. These actions can hence move towards structured comparisons between multiple scenarios and the joint analysis of their effects [29]. Therefore, further contribution to support the application of BBB principles would be reached [30–32]. In fact, although BBB is traditionally associated with post-disaster recovery and reconstruction its core concepts are highly relevant for preparedness-oriented assessments, since they stress the importance of (a) understanding multiscale interactions within urban systems, (b) integrating both social and physical dimensions, and (c) integrating the effects of dynamics on presence and behaviors of users [11,31,33–36]. In this sense, BBB also advocates for people-centred approaches, comprising alternative configurations of UBE use that may reduce vulnerabilities or improve risk management [33].

In view of the above, the following two research questions should be considered in UBE risk assessment and mitigation:

1. "How do different user factor conditions influence risk levels for the same SUOD?"
2. "How do different SUODs conditions affect the risk levels for the same user factor conditions?"

A multi-layer single-risk approach can be particularly suitable to face these questions [29]. In fact, it can synthetically analyse the intensity and spatial distribution of risks associated with different hazard sources in urban environments, especially when hazards coexist without directly interacting [37]. This methodology enables separate assessments for each hazard type, while ensuring comparability between scenarios through uniform analytical tools and consistent contextual conditions [38].

The multi-layer single-risk assessment approach could be applied to the multiple spatial scales which capture the variability and interactions of urban elements [39–42]. The microscale focuses on individual buildings and their immediate surroundings, focusing on detailed structural and functional characteristics, as well as their relationship with adjacent buildings and open spaces. On the opposite side, the macroscale addresses the urban system as a whole, including city size, spatial distribution of population and jobs, urban morphology, development patterns, and landscape connectivity, allowing the assessment of broader systemic resilience and city-wide interactions. Finally, the mesoscale represents an intermediate level encompassing public open spaces (such as streets, urban squares, riverfront promenades), as well as neighbourhoods and building blocks [4,43]. Therefore, the mesoscale is especially suitable for the aforementioned perspective in scenario creation and multi-layer single-risk assessment, since it captures dynamic patterns of UBE use, exposure, and vulnerability while maintaining sufficient detail to support targeted preparedness and mitigation strategies. In particular, considering short and long-term urban adaptation processes [9,25,43], focusing on public open spaces ensures analysing the minimum spatial units where users effectively move and gather under normal conditions, as well as where they behave and react during emergencies. Their physical characteristics, including size, accessibility, and adjacency to buildings, influence both hazard impacts and user exposure. Given the dynamics in user presence introduced above, the open spaces can significantly act as risk amplifiers, because high user densities can exacerbate risk by increasing potential losses during disasters [25].

In view of the above, this work aims at incorporating spatiotemporal use dynamics into urban risk assessment by adopting a multi-layer single-risk approach and an open-space-centred perspective in "what-if" scenario development. In line with the multi-layer single-risk approach [29], the methodology is applied to earthquake and flood through independent analysis (which means that no interaction and spatiotemporal relationships are considered). Hazard-specific urban hot spots can be identified, enabling a final comparison and integration of results across different risks thanks to a coherent and harmonised structure.

First, alternative scenarios in terms of user exposure and vulnerability are defined and elaborated to trace different use dynamics, representative of typical conditions in the fruition of the urban built environment. These scenarios explicitly account for temporal variability across hourly-based typical day periods, weekdays versus weekends, seasonal conditions and special-use periods, and are constructed based on the intended functions and regulatory temporalities of spaces, rather than on high-frequency population density data. Second, parameters on physical vulnerability and hazards are collected and combined, also allowing to consider the impacts of floods and earthquakes on the UBE. Boosting previous multiscale interaction perspective between interdependent sub-systems in urban areas [4,39,43], data on these risk factors are derived by organising building-related data (microscale analysis) for each open space to which they are linked (mesoscale assessment). Evaluations of risk scenarios are hence sensitive to both spatial configuration and spatiotemporal user dynamics, effectively bridging detailed microscale analyses and broader macroscale assessments.

Then, basic evaluations on these risk factors are combined to derive risk levels, which are indeed associated with the mesoscale representation of the UBE. These steps are elaborated by applying and adapting existing, consolidated methodologies, fostering rapid assessment techniques and ensuring reliable outputs [41,44–46]. The application to a historic UBE (a part of the old town of Senigallia, in Italy) demonstrates the approach capabilities in relevant real-world scenarios.

This work hence contributes to the development and showcasing of methods for the comparison, at the open space level, of single risk levels (1) for different spatiotemporal use dynamics under the same disaster conditions, and (2) for different disasters under the same spatiotemporal use conditions, in line with the two main research questions. In this process, the contribution hence lies in integrating spatiotemporal use dynamics, multi-risk assessment and mesoscale representation within a single, operational framework tailored to complex urban built environments. While the pursued standpoint aligns with recent advances in dynamic population modelling [21], the proposed approach also contributes to frame spatiotemporal variability of components within an overall hazard-agnostic structure, suitable for refinement an application to diverse risks, as well as to complex UBEs as historical ones [33,47].

Considering the work aims, Section 2 traces the background for the work, while Section 3 provides the assessment methodology. Then, Section 4 introduces the case study and provides an overview of the use dynamics considering the method application. Section 5 shows the case study application results, and Section 6 finally points out the main research key findings, limitations and needed future research steps.

2. Background

Understanding the role of urban public open spaces in this context allows the development of more effective methods for risk scenario creation and assessment, and to move towards multi-layer single risk assessment. On this basis, the pursued novel open-space-centred approach is framed through a targeted literature review focusing on: (1) the role of dynamic user factors in urban risk assessment (Section 2.1); (2) open-space-centred and mesoscale methodologies for scenario creation (Section 2.2); and (3) multi-layer single-risk assessment frameworks (Section 2.3). This structured review allows the proposed methodology to be clearly positioned within the relevant state of the art and clarifies its contribution with respect to existing approaches.

2.1. *The role of public open spaces for risk scenario creation and assessment*

Considering normal fruition, the public open spaces in the UBE, where the hosted population daily live, gather, move, and behave [25,48], represent the spatial units at which user exposure and vulnerability can be analysed as time-dependent and scenario-specific variables, rather than as static attributes. In fact, in case of an emergency, users respond to SUODs and activate immediate emergency behaviours by interaction with the elements of the open spaces [9,49,50]. In this sense, defining possible fruition scenarios becomes paramount to determine [41,51]: (a) how many users are present and where they are placed, contributing the definition of user exposure factors; and (b) identifying their typologies, in terms of gender, age, motion abilities, knowledge of the UBE/risks/emergency procedures, by then characterizing their individual vulnerability. Open spaces and their surrounding buildings are characterised by occupancy schedules per typology of intended use in indoor and outdoor areas, and which can also consider exceptional occupancy conditions (e.g., due to mass gatherings, touristic seasons) [41,52]. Occupancy variability contributes to the effective spatiotemporal distribution in the number and typology of exposed users, and thus affects the expected losses and casualties over UBE space and time [21,22,27,53,54].

Moreover, the organisation of public open spaces forms the foundation of the urban form and morphology, along with the structure and layout of neighbourhoods and blocks [40,43,55]. In this mesoscale and open-space-centred perspective, microscale data on risk factors should be collected considering each building facing a street or an urban square, and the outdoor areas hosted in the open space [41,43,56]. Then, such input data can be aggregated per open space, given its discretisation in the urban street network as an element limited by two nodes (crossroads, plano-altimetric variation). This allows to consider internal conditions as homogenous as possible. This mesoscale aggregation can also contribute to the macroscale level assessment tasks [4,57], by organising related results at the district levels, or even at the overall urban scale [58].

Recent studies highlight the need to apply these principles to historical UBEs, characterised by complex morphology, structural fragility, exposure to multiple hazards, and intense human activity, often amplified by tourism [41,59,60]. In view of these characteristics, comprehensive risk assessment in historical UBEs is more and more relevant, and represents a basic step to balance risk reduction strategies deployment and heritage conservation [41,61,62].

2.2. *Relevant approaches for flood and earthquake risk assessment at the public open space scale*

The Sendai Framework emphasises the importance of understanding disaster risk, strengthening risk-informed planning, and investing in disaster risk reduction to enhance preparedness and ensure more effective responses [7,32]. In this context, recent works highlighted the need to move beyond static representations of risk, explicitly acknowledging the role of exposure dynamics, social vulnerability, and spatial configurations in shaping disaster impacts [21,27,41]. These concepts share many similarities with people-centred approaches to disaster risk management promoted by the BBB principles [31,32]. While encouraging community involvement in planning and decision-making, BBB also promotes the exploration of alternative spatial and functional urban configurations to support risk reduction and mitigation. Therefore, it needs the deployment of structured frameworks for the inclusion of user dynamics in the whole assessment process, under different use conditions and their temporalities. Considering the mesoscale level (Section 2.1), preparedness activities can exploit related assessment results [33,61], to: (a) effectively design strategies depending on identified risk-sensitive open spaces; (b) anticipate the impacts of potential hazard scenarios; and (3) prioritise interventions that reduce vulnerability while respecting social and cultural values.

To support these actions, many previous studies investigated the role of public open spaces in UBEs under flood and earthquake scenarios, focusing initially on interactions between hazards and physical vulnerability factors [11,43,63–66]. For floods, hazard conditions can be described by different sources (e.g., fluvial, pluvial) and related scenarios in terms of return periods, including floodwater propagation in the urban fabric [36,67–69]. Physical vulnerability is defined by the morphology and construction of open spaces, infrastructure, and buildings, as well as mitigation measures, and thus it strongly influences flood impacts [70–75]. In the case of earthquakes, impacts depend on seismic events (e.g., peak ground acceleration at given return periods) and are influenced by building and infrastructure vulnerability, as well as urban morphology (e.g., dimension and plano-altimetric configuration) due to potential earthquake-induced debris [9,46,76–78].

Holistic scenario creation and risk assessment have also considered spatiotemporal dynamics of user presence, which affect response and evacuation conditions [11,21,24,27,41,79,80]. Public databases (such as statistics institutes, local authorities, census surveys) provide basic data on user numbers and vulnerability characteristics (e.g., age), but these are static and cannot capture daily, weekly, or seasonal variability [27]. Consequently, implementing daily and hourly profiles of user factors, considering public function timetables and mobility patterns (e.g., weekdays vs weekends), can improve scenario realism [21,22,25]. User numbers, and thus potential casualties, vary with exposure. For instance, nighttime earthquakes may have more casualties than daytime events, while roads and public buildings are more exposed during the day or on weekdays, as most individuals are likely to be indoors, at home [22,54]. On the contrary, road networks and public buildings will be more exposed during the daytime, due to visitors' presence. Furthermore, on weekdays, the concentration of users in urban areas and infrastructures increases exposure, while during holidays it tends to shift toward residential or recreational zones. These variations significantly influence both risk assessment and management [21].

The analysis of risk factors and the risk assessment can be carried out at several scales (see the Introduction). The macroscale allows rapid data collection and processing, using large areas in UBEs (e.g., based on GIS data aggregation) and grid-based techniques (ranging from the discretisation of UBEs of some tens of meters up to kilometres) [1,22,27,81,82]. The adoption of grid-based approaches enables the definition of quick-to-use maps of hot (and cold) spots, which can support decision-makers in the easy identification of critical UBEs parts, by also ensuring dynamic scenarios representation and comparison [22]. However, it could oversimplify user patterns in UBE, ignoring the contribution of conditions for the public open spaces. In contrast, the mesoscopic scale, applied in this study, allows a more detailed reading by capturing the interactions between UBE and users while remaining operationally feasible for urban-scale applications [39–41,43].

This approach has been used for earthquake [24,58,78] and flood [21,83] scenarios, often relying on microscale data to enhance detail [41,84]. Previous works in this direction widely exploited GIS sources, quick assessment methods or simulation-based tools, mainly oriented towards the definition of effects and damages in the UBE (e.g., floodwater modelling to define floodwater depths and speeds [49,85], building damage level and expected debris [86]). They support high-resolution outputs, capturing interactions among hazards, infrastructure, and user behaviour within narrowly defined spatial contexts, such as street segments, urban squares, or building fronts.

In this perspective, microscale GIS analyses integrate detailed spatial data (e.g., urban morphology, land use, building distribution) with modelling tools (e.g., 3D, hydraulic and structural models) to simulate realistic risk scenarios, such as flooding or earthquake-induced collapses, and identify vulnerable micro-areas [86]. These methods also support localised emergency management [42,87,88]. Nonetheless, most research linking micro and mesoscale analyses focuses on hazards and physical vulnerability, while few studies explicitly account for dynamic user exposure and its temporal variability within open-space-centred assessments. This remains a significant gap for preparedness-oriented risk scenario creation [41].

2.3. Connecting multi-layer single-risk assessment in UBE

Efforts to integrate flood and earthquake into multi-hazard risk modelling and assessment [29,89], risk management [90], loss assessment [91] and resilience analysis and mitigation [16,92] have been recently performed. These actions are based on the adoption of a common spatiotemporal framework, along with consistent indicators [16,29]. Furthermore, they should rely on the analysis of risk interactions due to hazard and vulnerability levels, also comprising events occurring simultaneously, sequentially, or in a cumulative way, that may generate cascading effects that exacerbate the overall impact on urban systems [29,93,94]. These interactions influence both hazard levels and the vulnerability of the exposed environment, making integrated risk modelling a complex task [95]. Due to these challenges, risks are often assessed independently, while still using harmonised assessment procedures and final metrics [37]. Indeed, applying a multi-layer single-risk approach can enhance integrated decision-making, provided that outputs use the same spatiotemporal resolution, which facilitates the comparison of results, maintaining the specificity of each hazard type [29]. Although it does not explicitly address hazard interactions [93], multi-layer single-risk assessment offers clear advantages for UBE planning, particularly when data availability is limited or hazard interdependencies are difficult to model. Moreover, this approach allows the stratification of multiple scenarios reflecting different UBE use patterns or hazard configurations, thereby supporting the exploration of combined effects of spatiotemporal variability in exposure and hazard intensity.

In this context, research has identified joint indicators for assessing resilience to floods and earthquakes [16,92]. These studies suggest that, given the same built environment and population characteristics, comparing indicators (e.g., Expected Annual Loss for floods and earthquakes) can help identify (1) the predominant risk in each part of the assessed area, and (2) "hot-spots" between them [29]. Similar approaches have been noted for other risks, including slow-onset ones, such as heatwaves and pollution [96]. However, these methods mainly address macroscale aspects and, when applied to UBEs, they consider population and land-use factors [16], but do not fully capture risk at the level of individual open spaces. This limitation can be addressed through harmonised single-risk assessments at a consistent mesoscale resolution [27,29,96]. In this sense, applying a multi-layer single-risk approach at the mesoscale allows systematic comparison of hazard scenarios under varying user conditions, reinforcing the role of open spaces as common reference units across layers.

As a final outcome, multi-layer single-risk approaches could also be applied to assess the co-benefits, trade-offs and maladaptation policies of possible measures aimed at separately reducing flood and earthquake risks [4,97,98]. In this way, they can extend the point of view from the one related to the combination between flood and other climate-change disasters.

3. Phases and methods

This research is organised in the following four main phases (comprising specific sub-sections in which related methods are reported), according to the workflow shown Fig. 1:

1. The *Data collection and organisation* (Section 3.1) is first performed by considering the identification of the public open space structures. Related data sources for database development have also been defined;
2. The *Users' Exposure and Vulnerability Assessment* (Section 3.2) comprises the spatiotemporal analysis of users' presence and typology, respectively, and is essentially based on the spatial location of functions in the UBE. Data are hence collected at the scale of each function hosted in the UBE, also considering the related occupancy schedules, first based on hourly periods. Then, data are aggregated for every single open space and organised into typical day periods (i.e., nighttime, morning, noon, afternoon, evening) to provide a quick overview of recurring conditions for the users' indexes. *Exposure* (*E*) is calculated uniformly across both flood and earthquake scenarios. Contrarily, *vulnerability indexes* (*UV*) consider common issues related to age and familiarity with the UBE, and disaster-specific parameters about the position of users in the UBE (i.e., indoor and outdoors);
3. The *Single-risk Physical Vulnerability and Hazard (PVH) Assessment* (Section 3.3) is performed considering the specificities of flood and earthquake scenarios. In this sense, building features and return periods used in the assessment process are firstly identified, to respectively evaluate the levels of building Physical Vulnerability (*PV*) and the Hazard (*H*). Then, data are aggregated at the open space level, and a matrix-based approach is proposed to determine the overall *PVH* level in terms of effects due to each assessed risk. The methodology distinguishes general parameters and criteria from risk-specific issues;
4. The *Multi-layer single-risk assessment* (Section 3.4) is finally aimed at combining *PVH*, *E* and *UV* to generate the final risk matrices, depending on the day period, on the public open space of reference, and on the selected risk scenario. The results are visualised through risk maps, useful to facilitate identification of worst-case emergency scenarios, hot-spots and the most critical open spaces in the study area, while also comparing flood and earthquake conditions.

This workflow is hence intentionally designed as a single-layer multi-risk approach [29]. Each risk is hence assessed under separate conditions, but through a coherent and harmonised structure ready for comparisons and results merging. More specifically, the approach maintains analogous procedures for user exposure and vulnerability, following consolidated mesoscale methods [41], ensuring direct comparability between flood and earthquake scenarios. Therefore, the workflow is ideally applicable to multiple hazards, adopting a hazard-agnostic structure for framing temporal variability in spatiotemporal user distribution and behavioural assumptions [47].

The workflow is then applied in this work to a relevant neighbourhood within the riverine historical UBE of Senigallia, Ancona, Italy, placed along the Adriatic seacoast and crossed by the Misa River, which has been introduced in the Case Study section (Section 4).

3.1. Data collection and organisation

The adopted methodology follows the mesoscale approach (see Section 2.2), according to validated methodologies for quick single risk assessment in UBEs [41].

In the first phase, all relevant data to characterise the study area are collected, comprising: UBE boundaries, buildings, public open spaces and their intended uses. Buildings are considered as both isolated units and structural aggregates, typical of historical UBEs [46]. Geometrical information (i.e., covered surface area and number of floors) can be obtained through, for instance, Google Maps, Street View and Calc Maps tools,[1] enabling remote surveys when GIS-based data are unavailable.[2] Moreover, constructive, material and structural data could be retrieved using remote surveys (e.g., using Google Maps, Street View or any updated photographic source), existing municipal databases or in-situ surveys.

An inventory of indoor and outdoor intended uses has been created. Each of them is associated with the related building and with the specific open space (street or square) based on the position of its entrance/access point. Then, the gross area is calculated by multiplying the covered surface area and the number of floors where the intended use is deployed. Each intended use is also classified

[1] https://www.google.it/maps; https://www.calcmaps.com/map-area/(last access: 15.05.2025).

[2] https://ottomilacensus.istat.it/sottotema/042/042045/2/(last access: 15.05.2025)[2] https://ottomilacensus.istat.it/sottotema/042/042045/2/ (last access: 15.05.2025)[2] https://ottomilacensus.istat.it/sottotema/042/042045/2/(last access: 15.05.2025).

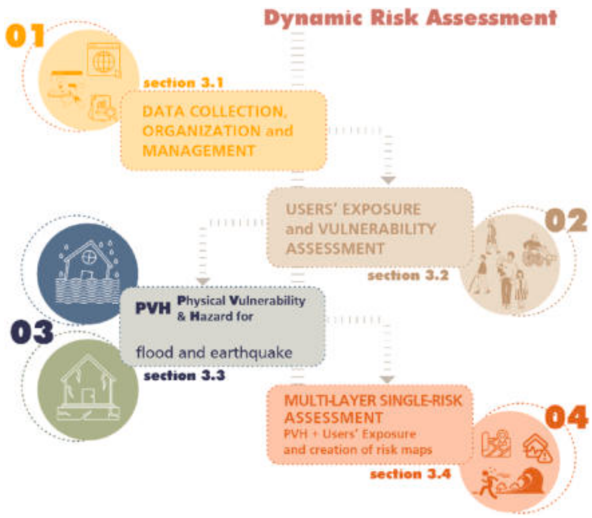

Fig. 1. Workflow of this research, including references to each section in which specific methods are discussed.

by floor and linked to an occupant load [persons/m^2] to estimate maximum potential user numbers. This allows the reconstruction of horizontal (indoor/outdoor) and vertical (floor-dependent) user distributions. For occupant loads, this study refers to the Italian Fire Prevention Code [99]. Opening and closing times are recorded for summer and winter to derive hourly occupancy schedules. These hourly schedules are then aggregated into typical day periods.

Outdoor areas hosting events or mass gatherings (e.g., fairs, exhibitions, festivals) are also identified. Then, additional occupancy load is assigned to these areas to represent seasonal conditions and specific events/mass gatherings, ranging from low (0.1-0.2 persons/m^2) to critical (i.e., 4 persons/m^2) density values, according to the Levels of Service (LOS) Theory [100]. Supplementary Material S1 provides a structured overview of these data for the case study. The proposed approach adopts standardised values and could provide overestimation in maximum crowding levels. Nevertheless, it ensures rapid applicability by decision-makers in real-world operational contexts and can support conservative assessment results, as also remarked by previous research [41].

Moreover, demographic information is collected at the whole UBE or city level from public statistical and census databases, including those freely available on public websites (for this study: Istat, 2023 census,– see Section 4). Main data concerns basic user typologies by age. The age categories considered in the analysis are: Toddlers (*T*), 0-4 years; Parent-assisted Children (*PC*), 5-14 years; Young Adults (*YA*), 15-19 years; Adult users (*AU*), 20-69 years; Elderly users (*EU*), 70 years and older. The percentage of users by age category is retrieved from these available statistical databases.

Finally, all data are organised according to the UBE road network, and consider that each public open spaces are represented as a link between two adjacent nodes (e.g., crossroads, plano-altimetric variations of the road network). Therefore, indoor and outdoor uses are linked to the open space they face or occupy, enabling spatially consistent representation of user exposure.

3.2. *User exposure and vulnerability*

User exposure and vulnerability are assessed using mesoscale methodologies [41], which rely on the approach for spatial data collection and organization defined in Section 3.1.

User locations within the UBE are defined according to the two main categories of spaces (i.e., indoor and outdoor), described in Section 3.1. Indoor areas include residential buildings, commercial spaces, public and private services, and institutional facilities. They accommodate *indoor users*, both *residents* (*R*) and *non-residents* (*NR*). Outdoor areas include carriageways, parking lots, sidewalks, dehors and courtyards (excluding non-walkable surfaces), and they host *prevalent outdoor users* (*PO*), such as customers of shopping areas, bars and restaurants, and *only-outdoor users* (*OO*), such as passers-by.

According to reference works [41], this categorisation of space and user types is relevant both for assessing familiarity with the built environment, and for capturing temporal variation in user exposure and age-based vulnerability.

Residents are assumed to be fully familiar with the UBE and aware of its risks. The following assumptions are considered to trace their temporal framing at home, depending on age and typical home occupancy schedules. Toddlers and elderly individuals are assumed to remain at home due to limited or no mobility. Parent-assisted children and young adults are away from home (i.e., at school) between 8:00 and 13:00. Adults are away for working/studying activities from 8:00 to 18:00. Moreover, unemployed adults are assumed to remain in indoor residential spaces during typical working hours. The number of unemployed adults is rapidly calculated considering the percentage of unemployed adults in the UBE, according to the demographic databases selected in Section 3.1.

Non-residents, prevalent outdoor users and *only-outdoor users* are conservatively treated as non-familiar users, being unaware of possible risk conditions. The presence of *NR* and *PO* depends on the opening hours of the related public functions, respectively indoors and outdoors. Since opening times of public functions vary by weekdays, weekends and seasons, different scenarios can be created using the same methodology. In this way, *NR* and *PO* include commuters, day visitors and occasional users accessing these functions (regardless of their place of residence), and do not rely on official resident population statistics, but on regulatory occupancy loads, according to Section 3.1 assumptions. Additionally, critical scenarios, such as mass gathering events (identified as in Section 3.1), account for extra occupant loads. These users are classified as *PO*, and their presence depends on event timings. Conversely, a simplified temporal framing is assumed for *OO*. They are considered present from 07:00 to 24:00 and absent during nighttime.

Intersecting schedules of public and private spaces on an hourly-based scale, it is possible to derive the spatiotemporal distribution of users per intended use in indoor and outdoor areas. Then, it is possible to perform their mesoscale aggregation per public open space. The calculation of time-dependent *user exposure E* [−] and *user vulnerability UV* [−] parameters is then provided on these bases, with respect to general (Sections 3.2.1) and risk-specific issues (Section 3.2.2). According to the general rationale of this work, these indices are defined to be normalised factors, thus numerically ranging between 0 (generally excluded in the presence of users, but included in case of abandoned places, i.e., open spaces) and 1 (as the maximum factor value).

3.2.1. General assessment methods

The user exposure *E* is assessed in all the hazard conditions according to validated methods at the mesoscale [41], as shown in Equation (1):

$$E = \frac{\left\{ \left[\sum_{ind} (R_{ind} + NR_{ind}) + \sum_{out} (OO_{out} + PO_{out}) \right] \Big/ A_{os} \right\}}{OL_{max}} = \frac{\{TOT_{users} \, / \, A_{os}\}}{OL_{max}} \tag{1}$$

where: *R* and *NR* refer to the related indoor intended uses *ind*, while *OO* and *PO* refer to the outdoor intended uses *out*, so at to calculated the sum of all the users of the OS (TOT_{users}) [persons]; A_{OS} is the outdoor surface area of the OS [m^2]; and $OL_{max} = 4$ persons/m^2 is the maximum acceptable occupant load for user permanence in outdoors, in emergency conditions (i.e., referring to LOS F). The outdoor surface area is used for normalisation because the indicator focuses on crowding levels in open spaces, which are critical for emergency gathering and evacuation. At the same time, during SUODs, people located indoors can rapidly move toward adjacent open spaces, thereby contributing to possible outdoor crowding levels [41]. This approach ensures that *E* represents a worst-case but realistic estimate of outdoor crowding, supporting preparedness planning and scenario-based decision-making at the meso-scale.

The *user vulnerability UV*, as previously outlined, is influenced by physical characteristics of the individual (i.e., age), behavioural aspects (i.e., familiarity with the UBE) and spatial positioning, both vertically (building floor level) and horizontally (location in open or built spaces) [21,22,27,51]. For these reasons, vulnerability is disaggregated into three parameters, according to previous approaches [41].

UVa represents the user vulnerability by age, estimated through Equation (2). Toddlers, parent-assisted children and elderly individuals are considered the most vulnerable categories due to their possible limited autonomy in both movement and decision-making.

$$UVa = (T + PC + EU) \, / \, TOT_{users} \tag{2}$$

UVf accounts for user vulnerability by familiarity with the UBE and its typical risks, computed through Equation (3). It reflects the proportion of users with low familiarity who can be associated with OO, PO and NR.

$$UVf = (OO + PO + NR) \, / \, TOT_{users} \tag{3}$$

UVp refers to the user vulnerability depending on their position in the UBE before the emergency conditions appear. Considering the different phenomenology of floods and earthquakes, *UVp* needs disaster-specific assessment methods, thus reported in Section 3.2.2.

3.2.2. Risk-specific assessment methods

In flood emergencies, the main users exposed to risk are those located at ground floors of each building, and outdoors, as these spaces are directly affected by rising water levels [45,59,72]. Therefore, the user vulnerability to flood depending on their position UVp_f [−] should consider the number of users placed at the ground floor (*GFu*) [persons] along with *OO* and *PO*, as shown by Equation (4).

$$UVp_f = (GFu + OO + PO) \Big/ TOT_{users} \tag{4}$$

In earthquake scenarios, users exposed to risk mainly include all individuals located within buildings, and thus indoors, regardless of floor level, encompassing both *R* and *NR* [22,79]. Therefore, the user vulnerability to earthquake depending on their position UVp_e [−] is calculated through Equation (5).

$$UVp_e = (R + NR) \, / \, TOT_{users} \tag{5}$$

3.3. Physical vulnerability, hazard and their combined impact

Section 3.3.1 traces general criteria for assessing *PV*, *H* and their combination, moving towards the aforementioned hazard-agnostic standpoint. Nevertheless, *PV* and *H* are disaster-specific: Section 3.3.2 defines *PVH* in flood scenarios [44,45], while Section 3.3.3 assess *PVH* in earthquake scenarios [46].

3.3.1. General assessment criteria

According to common issues in basic disaster-specific calculation methodologies and rapid risk assessment and management approaches [37,45,46,101], the process of *PVH* assessment in flood and earthquake scenarios essentially relies on the following basic concepts:

- *PV* characterises buildings in terms of their material, structural, geometrical, damage and conservation features, which determine their predisposition to damage under a given hazard intensity. In this context, “damage features” refer to pre-existing deficiencies or observable conditions (e.g., cracks, material degradation, or general state of conservation) that affect the building current structural capacity. These features are commonly included in rapid vulnerability assessment methods. Each building has its own *PV* value, considered constant in all the scenarios. These features can generally be evaluated through remote surveys (see Section 3.1), although some uncertainties may require a scenario-based approach, selecting different reference conditions (i.e., for earthquakes, see Section 3.3.3 discussion);
- *H* represents the severity of the disaster event according to its basic components (i.e. floodwater depth [m] and speed [m/s] for floods; Peak Ground Acceleration [g] for earthquakes). Different scenarios for floods and earthquakes describe varying severity levels depending on boundary and return period conditions. To pursue a rapid assessment, in each given scenario, *H* is assumed homogeneous for all the buildings, and for the entire historical UBE. Nevertheless, the same methodology could be applied, considering local amplification/reduction factors of hazard at meso and microscales;
- *PV* is combined with *H* using a matrix-based approach to ensure quick application by decision makers and their technicians. Each *PV-H* combination corresponds to a *PVH* value expressed in terms of possible effects (damage or consequences), using discrete classes of values which range from negligible to extreme. *PVH* is calculated for each building. The *PVH* class for each public open space is the most frequent value among its facing buildings, weighted by the building gross covered area. Therefore, while *PV* remains constant across scenarios, *PVH* varies depending on hazard severity and expresses the scenario-dependent damage potential. The higher the *PVH*, the higher the damage status of buildings, as well as the higher the effects on the facing open space, due to direct building damage effects (i.e., for earthquakes and floods) and to outdoor emergency conditions (i.e., considering flood in terms of floodwater depth and speed).

Finally, the open space-related *PVH* will vary in the range 0 to 1, as the maximum value, as for *E* and *UV* values, to ensure comparability in the final risk assessment process.

3.3.2. Flood-specific parameters and assessment

Flood conditions are assessed according to the integration of previously validated methodologies [44,45].

H is expressed in terms of the Flood Hazard Index (*FHI*) [m^2*s], while *PV* is expressed in terms of Flood Vulnerability Index, *Ivf* [−]. Then, *PVH* is given by the combination of *H*=*FHI* and *PV*=*Ivf* according to the matrix provided in Fig. 2.

In particular, *FHI* is computed as a function of water depth [m] and speed [m/s], as shown in Equation (6). Five related classes of values are then identified for the matrix-based assessment application, as shown in Fig. 2.

$$FHI = depth \cdot (speed + 0.5) \tag{6}$$

Ivf is calculated using a simplified index-based method that combines *Exposure Index* (*EI*) and *Sensitivity Index* (*SI*) [−]. The calculation of these indicators is adapted from the validated methods [44,45] to reflect the specific context and physical characteristics of the case study application in an Italian historical UBE. *EI* is based on a single parameter (i.e., wall orientation [44]) as the main leading factor in view of quick application to riverine UBEs. This parameter evaluates the susceptibility of the building based on the orientation of its main façade with respect to flood flow direction. Thus, the direction of floodwater spreading and flow across the UBE

Flood PVH			Hazard [H=FHI]				
			Negligible [H≤0.75]	Low [0.75<H≤1.25]	Moderate [1.25<H≤2.5]	High [2.5<H≤7.0]	Extreme [H>7.0]
Flood Vulnerability Index *Ivf*	Extreme	75 < Ivf ≤ 100	Moderate	High	Extreme	Extreme	Extreme
	High	50 < Ivf ≤ 75	Low	Moderate	High	Extreme	Extreme
	Moderate	25 < Ivf ≤ 50	Low	Low	Moderate	High	Extreme
	Low	Ivf ≤ 25	Negligibile	Low	Low	Moderate	High

Fig. 2. General flood risk matrix: combination of hazard and physical vulnerability (PVH).

can be assumed to create different hazard scenarios, characterised by the same *FHI* classes defined above. Considering riverine contexts as the application one, the main scenarios could relate to floodwaters spreading parallel and perpendicular to the river axis, as opposite conditions [59]. The wall orientation is categorised into four classes:

- Class A: Partially exposed, no openings;
- Class B: Partially exposed, with openings;
- Class C: Fully exposed, no openings;
- Class D: Fully exposed, with openings.

EI could also be evaluated by including the parameters considered in other reference works [45]. Nevertheless, in this work, the type and use of activity are directly included in the *E* and *UV* assessment. The surface condition is assumed to be constant, as the analysed UBE refers to a homogeneous floodplain context. Hence, the heritage value is included in *SI*, considering the intrinsic feature of the building [44].

SI is composed of seven parameters to integrate reference methods [44,45], each associated with four vulnerability classes (A-D), as follows:

- Structural materials (A = steel/reinforced concrete, B = masonry, C = timber, D = earth);
- State of conservation (A = good, B = slight existing damage, including minor cracking and moisture, C = generalised existing damage, including cracking, and erosion, D = serious decay and expressive cracking);
- Number of floors (A = one, B = two, C = three, D = four or more);
- Age (A = 21st century, B = from 20th to 21st century, C = from 15th to 20 to century, D = older than 15th century);
- Heritage status (A and B = unclassified, C = national interest and protection, D = international interest and protection);
- Façade materials (A = steel/concrete/glass, B = brick/plaster/regular dressed stone, C = unglazed tile/irregular stone/wood panels, D = adobe or rubble stone);
- Window/door frames at ground floor (A = plastic, B = metals, C = wood, D = fully exposed and thus without frames).

The existence of basement and door threshold height, proposed in previous research [45], could still be included to calculate *SI*, but they are here excluded due to their poor relevance in the application context, with homogenous conditions referring to a negligible vulnerable configuration of this parameter. Conversely, openings at ground level (considered in Ref. [45]) are instead covered by the wall orientation parameter under *EI*.

Each class in *EI* and *SI* is associated with an increasing value: A = 10, B = 40, C = 70, D = 100. The final sensitivity score is obtained by summing the scores from the related parameters, while *Ivf* is then calculated as shown in Equation (7), obtaining a normalised value ranging from 0 to 100:

$$Ivf = \frac{(EI \cdot SI) - (EI_{min} \cdot SI_{min})}{(EI_{max} \cdot SI_{max}) - (EI_{min} \cdot SI_{min})} \cdot 100 = \frac{(EI \cdot SI) - (10 \cdot 70)}{(100 \cdot 700) - (10 \cdot 70)} \cdot 100 = \frac{(EI \cdot SI) - 700}{70000 - 700} \cdot 100 \tag{7}$$

where *min* and *max* respectively refer to the minimum and maximum values of *EI* and *SI*, which are also numerically shown in Equation (7). Then, *Ivf* is divided into classes according to Fig. 2. Considering mainly two floodwater spreading scenarios, two *EI* values are retrieved, and then two *Ivf* values are calculated, indeed one for parallel and one for perpendicular flow directions.

Finally, the flood *PVH* index, resulting from the matrix-based combination between *H*=*FHI* and *PV*=*Ivf* as shown in Fig. 2, is divided into five hazard levels (negligible to extreme), associated to numerical values to ensure their application in the risk assessment metrics defined in Section 3.4: negligible, 0.2; low, 0.4; moderate, 0.6; high, 0.8; extreme, 1.0. The “negligible” class is associated with *PVH* = 0.2 to capture potential operational impacts on public spaces, rather than representing an absolute “dry/no-effect” state (which would ideally imply *PVH* = 0). This choice reflects a conservative, application-oriented approach: even minimal flood conditions (small depth, low speed, or partially sheltered façades) can affect open-space usability, accessibility, and user safety.

3.3.3. Earthquake-specific parameters and assessment

Earthquake conditions are assessed according to previous validated methods [46], which are consistent with the Italian application context of the case study.

H is expressed by the return periods [years] according to the site hazard provided by national seismic hazard maps, which report Peak Ground Acceleration (*PGA*) [g] on the Italian territory at the city level [102]. Four return periods are selected to represent *H* corresponding to the Limit States defined by the Italian Building Code [103], and to typical damage grades of the EMS-98 scale [104]. 50-years and 101-years return periods refer to two Damage Limit State, respectively considering negligible to slight damage for structural/non-structural elements (without impact on user safety or building resistance) and light damages to very few walls (e.g., light cracks; fall of small or fairly pieces of plaster; fall of loose stones from the upper parts of buildings; partial collapse of chimneys). These conditions can be generally associated with D0, D1 and D2 damage grades in EMS-98. The 475-year return period refers to Life Safety Limit State, and implies moderate damage to non-structural elements (from cracks and partial falls, up to roof tiles detach, chimneys fracture at the roof line, and failure of individual partitions and gable walls), and substantial damage to structural elements, with loss of stiffness to horizontal forces, moving towards possible subsequent collapse conditions. This return period can be associated with D2 and D3 grades in EMS-98. Finally, the 975-year return period refers to Collapse Limit State (CLS), implying serious damage to non-structural elements, very heavy damage to structural elements and total/near-total collapse, essentially corresponding to D4 and D5 grades in EMS-98.

PV is expressed by the *Seismic Vulnerability Index* (*Ivs*) [−] [105]. *Ivs* is determined as shown in Equation (8) by the combination of:

- basic parameters, each having a specific weight w_i [−] depending on its importance in the whole *PV* assessment; and a coefficient c_i depending on the type of parameter conditions, as shown in Table 1. Each coefficient is assigned to a class representing increasing vulnerability (A, B, C, D);
- the status of conservation k_1 [-], equal to 1.00 in the absence of cracks, to 1.05 in case of minor out-of-plane cracks, and to 1.10 in case of many cracks;
- the presence of anti-seismic devices k_2 [-]. Anti-seismic devices are applied to the building with the aim of improving its seismic performance, mainly by preventing the out-of-plain failures of buildings. They do not only comprise aseismic devices (e.g., buttresses) [106], but also seismic retrofitting solutions (e.g., stainless-steel ties). k_2 is classified depending on:
  - o no anti-seismic devices: equal to 1;
  - o anti-seismic devices with poor performance levels[3]: presence of anti-seismic devices on all floors, equal to 0.55; devices at the top and in floor n-1, equal to 0.65; devices at the top or in floor n-1 or n-2, equal to 0.85;
  - o anti-seismic devices with good performance levels and effective position: presence of anti-seismic devices on all floors, equal to 0.26; at the top and in floor n-1, equal to 0.31; at the top or in floor n-1 or n-2, equal to 0.43.

$$Ivs = \frac{\left(\sum_i c_i \cdot w_i\right) \cdot k_1 \cdot k_2}{100} \tag{8}$$

This work assumes that roof types and the effectiveness of anti-seismic devices could be affected by relevant uncertainties due to the possible lack of detailed analysis. Therefore, different vulnerability scenarios, "C", are proposed based on the following combinations of characteristic parameters, homogeneously assigned to all the buildings, as opposite scenarios:

- C1: sloped/pitched roof, considering the complete effectiveness of wall-to-roof connections in non-pushing roofs + anti-seismic devices with poor performance levels;
- C2: sloped/pitched roof, considering the complete effectiveness of wall-to-roof connections in non-pushing roofs + anti-seismic devices with good performance levels and effective position;
- C3: pushing sloped/pitched roof + anti-seismic devices with poor performance levels;
- C4: pushing sloped/pitched roof + anti-seismic devices with good performance levels and effective position.

In these scenarios, a "pushing roof" refers to conditions in which "the thrust is transferred to the top of the façade wall" [105]. These conditions negatively affect the building seismic response because "the horizontal action due to vertical loads are added to the horizontal seismic action", and because "the vertical seismic component increases the horizontal thrust" [105].

In view of the proposed seismic assessment method, each building is characterised by its *Ivs* for each of these vulnerability scenarios, being then classified into three categories, as shown in Fig. 3. Furthermore, each vulnerability scenario, characterised by a specific building *Ivs*, is developed around the four return periods representing *H*, within the damage matrix offered by Fig. 3 [46]. This results in a total of sixteen final values of the earthquake *PVH* index, which provide the probability of a building being damaged at increasing return periods in terms of damage grade. This deterministic structure does not aim to capture the full variability of damage across buildings, but provides a rapid, consistent, and operational tool for meso-scale assessment, suitable for historical UBEs composed of traditional unreinforced masonry [46,105].

The damage levels resulting from the damage matrix correspond to the EMS-98 scale, each of them associated with a numerical value to ensure their application in the risk assessment metrics defined in Section 3.4:

- D0: *PVH* = 0, no damage. This class represents no effects of the building damage on the facing open space (e.g., no debris). It hence provides a clear and consistent baseline for damage assessment, ensuring that only damaged buildings contribute to open-space risk evaluation
- D1: *PVH* = 0.2, negligible to slight damage, comprising no structural damage and slight non-structural damage;
- D2: *PVH* = 0.4, moderate damage, comprising slight structural damage and moderate non-structural damage;
- D3: *PVH* = 0.6, substantial to heavy damage, comprising moderate structural damage and heavy non-structural damage;
- D4: *PVH* = 0.8, very heavy damage, comprising heavy structural damage, very heavy non-structural damage (i.e., serious failure of walls, partial structural failure of roofs and floors);
- D5: *PVH* = 1.0, destruction, with very heavy structural damage leading to total or near-total collapse.

3.4. Risk assessment metric and mapping

The single-risk assessment metric *R* for each given open space in the UBE [−] is calculated as a weighted linear aggregation of

[3] Poor devices refer, for example, to stainless-steel ties not well distributed within the façade, under-dimensioned or deteriorated.

Table 1
Parameters for the *Ivs* assessment. *: this value is operationally assumed for sloped/pitched roofs, considering the complete effectiveness of wall-to-roof connections in non-pushing roofs, so as to amplify the representation of low-PV conditions.

w_i	Number of floors		Specific Weight [kN/m^3]		Slimness		Roof Type		Openings	
	29.69		8.59		30.08		22.66		8.98	
class	type	c_i	type	c_i	type	c_i	type	c_i	type	c_i
A	1	0.25	≥23	0.76	9	0.23	flat*	0	≤4%	0.54
B	2	0.36	20 ≤ sw ≤ 22	0.80	10 ≤ s ≤ 12	0.30	non-pushing	0.42	5% ≤ o ≤ 10%	0.77
C	3	0.52	17 ≤ sw ≤ 19	0.83	13 ≤ s ≤ 17	0.49	slightly-pushing	0.59	11% ≤ o ≤ 18%	0.88
D	>3	1.00	11 ≤ sw ≤ 16	1.00	≥18	1.00	pushing	1.00	>18%	1.00

Earthquake PVH			Hazard [Retun Periods (years)] [50]	[101]	[475]	[975]
Seismic Vulnerability Index *Ivs*	Low	Ivs < 0.55	D0	D1	D2	D3
	Moderate	0.55 ≤ Ivs < 0.70	D1	D2	D3	D4
	High	Ivs ≥ 0.70	D2	D3	D4	D5

Fig. 3. Damage matrix.

independently derived and normalised indices, thus according to a Weighted Linear Combination Method [75]. R hence depends on each specific and conceptually distinct component of disaster risk, as shown in Equation (9):

$$R = w_{PVH} \times PVH + w_{UVp} \times UVp + w_{UVa} \times UVa + w_{UVf} \times UVf + w_E \times E \tag{9}$$

where w_i [−] is the weight of each risk factor, representing its relative importance.

Equation (9) is applied separately to flood and earthquake scenarios, yielding two single-risk metrics in line with the adopted multi-layer single-risk approach [29,37]. While *E, UVa,* and *UVf* remain unchanged across scenarios, *PVH* is defined separately for floods (Section 3.3.2, Fig. 2) and earthquakes (Section 3.3.3, Fig. 3). In fact, *PVH* captures the probability of physical damage conditional on hazard type and intensity. Similarly, *UVp* is hazard-specific, as discussed in Section 3.2.2, since it represents the proportion of users directly exposed to risk depending on their position.

R ranges from 0 (no risk, due to the absence of users) to 1 (maximum risk) since *PVH*, *UV* and *E* components are discretised into consistent classes, and normalised to the [0,1] range. Normalisation ensures comparability among heterogeneous indicators with different units, scales, and uncertainty sources, enabling transparent and reproducible aggregation in multi-dimensional risk assessments.

The weights w_i associated to each component in Equation (9) are computed using the Analytic Hierarchy Process (AHP) [107,108], adopting distinct weighting schemes for flood and earthquake scenarios. AHP is a decision-support method that derives relative weights through pairwise comparisons based on a linear integer scale from 1 (equal importance) to 9 (extreme importance). Weights are calculated using the Row Geometric Mean Method (RGMM), ensuring that priorities sum to one for each risk assessment, while the Consistency Ratio (CR) is required to be below 10% to validate the comparisons. This approach combines qualitative expert judgment with quantitative processing, supporting complex decision-making while ensuring consistent and comparable results [75,109,110]. Following consolidated methods [41], experts in flood and earthquake risk assessment and mitigation from the Polytechnical University of Marche (Italy) were asked to independently perform the AHP procedure using consolidated Excel tools [108]. Individual judgments were then aggregated into a consensus matrix [111]. The consensus group included eleven participants for floods and eight for earthquakes.

The results of the AHP process are shown in Fig. 4 for flood scenarios and Fig. 5 for earthquake scenarios. In both figures, panel A reports the comparison matrix, while panel B presents the resulting weights (using columns to trace the mean values, and vertical bars as standard deviations due to the aggregation of results from the consensus group). The simplified matrix structure reflects the synthesis of expert judgments rather than a simplification of the methodological framework. The AHP matrices represent a static, expert-based weighting scheme, as commonly adopted in AHP applications, and are not intended to explicitly model temporal dynamics [75,109,110]. Nevertheless, the proposed framework still traces time- and scenario-dependent variability of the input variables (*E*, *UVa*, *UVf*, *UVp*, and *PVH*) to which the AHP-derived weights are applied in Equation (9). This allows the resulting risk index R to vary across scenarios and, mainly, in a dynamic way over time, while maintaining methodological consistency.

Given the above, the use of linear aggregation is motivated by its transparency and decision-oriented nature, as it enables rapid comparison and prioritisation across multiple open spaces, hazard scenarios, and time slots, supporting preparedness planning and risk mitigation rather than statistical prediction. In fact, such index-based aggregation approaches are widely adopted in multi-hazard and

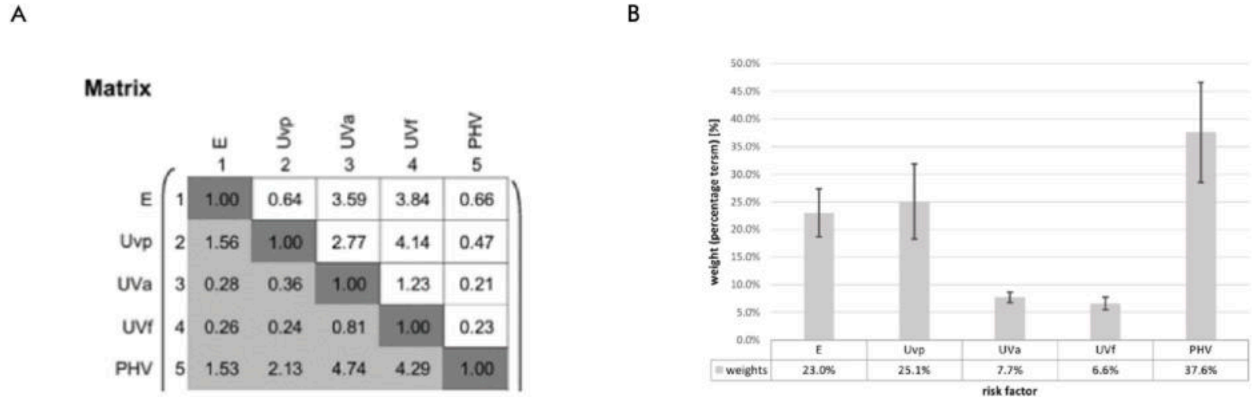

Fig. 4. Results of the flood-related AHP process: A-AHP comparison matrix; B-risk factors and related weights (columns), and vertical bars representing weight uncertainties (standard deviation).

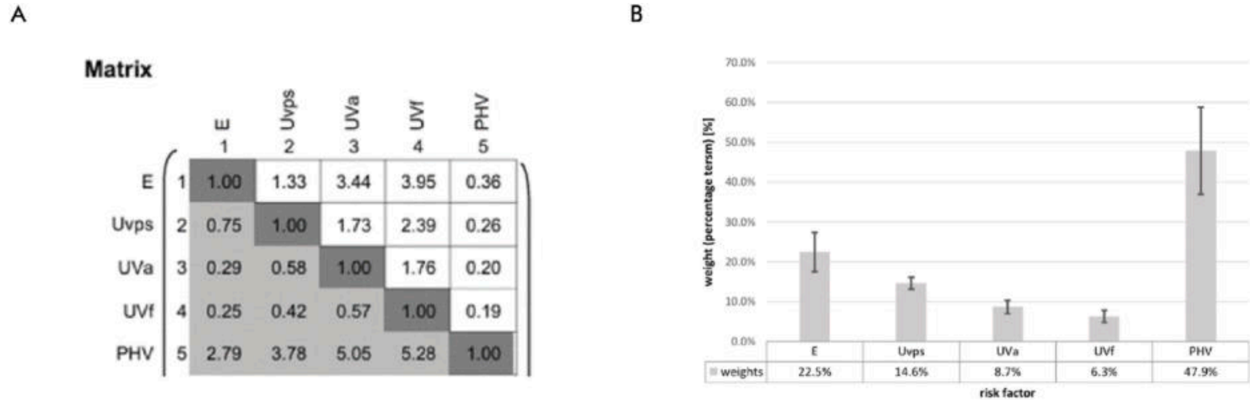

Fig. 5. Results of the earthquake-related AHP process: A-AHP comparison matrix; B-risk factors and related weights (columns), and vertical bars representing weight uncertainties (standard deviation).

multi-risk assessment, as well as in resilience studies, because they allow combining heterogeneous risk components, each characterised by different scales, units, and sources of uncertainty, in a transparent, interpretable, and reproducible way [29]. Second, the linear aggregation moves towards a direct decision-maker's support in outputs interpretability, since each index is associated with a simple weight [41,75,109,110]. Basic values of *PVH*, *UV* and *E* are thus directly connected to the final risk levels for each open space. It provides a clear ranking of open spaces, making it easy to communicate, and ensures direct comparison across multiple scenarios (hazard severities, use temporalities and conditions). Therefore, it also allows decision-makers to identify priority areas for interventions or emergency planning, which is the primary objective of our work, rather than performing statistical prediction. Moreover, for a meso-scale urban context, where rapid assessment across multiple open spaces and scenarios could be very useful, this index-based aggregation can also offer efficiency in data organisation.

E, *UV*, *PVH* and *R,* are then shown using maps visualisation, by classifying them into five categories of increasing into five levels of risk:

- Negligible = $0 <$ index <0.2;
- Low = $0.2 \leq$ index <0.4;
- Moderate = $0.4 \leq$ index <0.6;
- High = $0.6 \leq$ index <0.8;
- Extreme = $0.8 \leq$ index ≤ 1.

In particular, *R* can be used for assessing single-risk conditions (Section 3.4.1) and multi-risk conditions (Section 3.4.2), to support comparisons among flood and earthquake scenarios. In both cases, maps ensure a rapid visualisation of data for decision-makers, supporting them in identifying the most critical open spaces in the UBE, as well as the most critical times of the day.

3.4.1. Single-risk assessment criteria

In single-risk assessment, specific maps of *R* are provided by combining:

1. Each time of the day, spatiotemporal characterisation of *E* and *UV* factors (see Section 3.2);
2. Each disaster-specific scenario, and thus:
   a. For flood, given the specific *PV* conditions, distinguishing floodwater flow parallel and perpendicular to the river axis, additionally considering that each of them can have five *H* levels (negligible to extreme – see Section 3.3.2);
   b. For earthquake, distinguishing four scenarios (C1, C2, C3, C4) affecting *PV* values at the building level, additionally considering that each of them can be assessed by four return periods (50, 101, 475 and 975 years) representing alternative *H* conditions.

As an output, for each of the five daily periods defined in Section 3.2, 10 scenarios can be provided for flood emergencies, and 16 for earthquake emergencies. Therefore, different maps over time support the analysis for each of these scenarios.

3.4.2. Multi-risk comparison criteria

Multi-risk comparison is intended to support the analysis of the relative significance of flood and earthquake risk within the study area, according to previous approaches [29]. The Risk Ratio *RR* [−] is hence proposed, according to Equation (10), still focusing on each urban open space, providing a decision-support tool for prioritising mitigation actions:

$$RR = \frac{R_{FLOOD}}{R_{EARTHQUAKE}} \tag{10}$$

In Equation (10), R_{FLOOD} and $R_{EARTHQUAKE}$ are the risk values calculated for each hazard according to Equation (9) and its specific disaster-specific weights.

As a comparative indicator, *RR* allows for the identification of areas where one hazard represents a more significant threat than the other. Values of $RR > 1$ indicate greater flood risk, while values of $RR < 1$ point to a predominance of earthquake risk. This normalised approach supports a nuanced interpretation of risk patterns and offers valuable guidance for site-specific emergency planning and hazard mitigation strategies, oriented towards the prioritisation towards flood and earthquake depending on the *RR* value related to each open space. As for the other risk factors and metrics, *RR* is also visualised using maps-over-time, and considering the different scenarios defined in Section 3.4.1, as a combination of *PVH*, *E* and *UV* values.

4. Case study

Senigallia is a seaside city located in the Marche region of Italy crossed by the Misa River and populated by approximately 44,000 people. The city was the first Roman colony on the Adriatic coast and holds significant historical, architectural and geographical importance. Senigallia boasts a rich cultural heritage, including building heritage with national interest and protection, such as the “Rocca Roveresca” and “Palazzo del Duca”, built during the Medieval period, the “Portici Ercolani”, and the “Foro Annonario”, a historic market area along the Misa River.

The city has experienced damage from natural disasters such as floods and earthquakes over the years, which highlight the critical role of public open spaces in the distribution and intensity of risk in this UBE:

- For flood events, public open spaces located near the Misa River have historically suffered the most during flooding episodes. Notably, the floods of 2014, September 2022, and 2024 inundated streets, squares, and riverfront promenades, often causing partial damage to adjacent historic buildings. These events demonstrate how the location, morphology, and connectivity of open spaces near the Misa River can significantly influence both exposure and potential consequences for users. These incidents have also underscored the urgent need for the implementation of flood risk mitigation plans;
- For seismic events,[4] the most severe earthquake recorded in Senigallia occurred in 1930, resulting in the collapse of portions of buildings and impacting nearby streets and squares. The last events occurred in 2022, which caused relevant disruptions, although localised, and no casualties. All these events consistently highlighted the vulnerability of historical buildings adjacent to open spaces and the role these areas play in evacuation, emergency access, and temporary sheltering.

In addition, Senigallia is one of the most relevant tourist destinations in the Marche Region, as well as along the Adriatic coast, with more than 100 beds/km^2 (which means more than +25% of the exposed population, considering a resident density of about 370 persons/km^2).[5] Moreover, it is renowned for the international music and cultural festival known as Summer Jamboree,[6] which takes place in the seafront and in the historical city centre, creating a temporary and relevant increase in the population (more the 5 times the residential population). Most of the related public events are also generally hosted outdoors. Therefore, due to the combined presence of tourists for holidays and specific mass gatherings, the high intensity in terms of temporary user exposure makes Senigallia an ideal case study for the joint challenge of local heritage valorisation and risk management.

Fig. 6 describes the historic UBE of Senigallia chosen as the case study application, considering the adjacency with the Misa River

[4] https://emidius.mi.ingv.it/CPTI15-DBMI15/query_eq/(last access: 13.08.2025).

[5] https://statistica.regione.marche.it/Marche-in-Numeri/Turismo; https://statistica.regione.marche.it/Portals/0/Enti/42045_Senigallia.pdf (last access: 13.08.2025).

[6] https://www.feelsenigallia.it/en/(last access: 13.08.2025).

Fig. 6. Identification of the whole historic centre of Senigallia, along with the specific study area (a), and of buildings and open spaces in the analysed UBE (b).

(in blue). In particular, the selected areas are those comprising the main building heritage and the streets and urban squares hosting mass gatherings all over the year. Fig. 6a shows the whole historic town boundaries, and the part investigated in the following (marked in red). Fig. 6b offers the organisation of the case study area into buildings, and the open spaces, identifying the links and nodes along with the specific codes used in the following in association with each street and urban square. Most of the open spaces are pedestrian areas, except for the riverside avenue, which is usually open to vehicular traffic, apart from mass gathering conditions. The areas that host mass gatherings are highlighted in Fig. 7c.

In addition to Google Maps and Google Street View surveys, buildings and open spaces have been surveyed using architectural interventions planning by the Municipality of Senigallia.[7] The documents also reported updated visualisation and data of façades and plans. These sources have been also used for the identification of the activities hosted in the study area (Fig. 7), in particular the residential function (Fig. 7a), and public intended uses (Fig. 7b), such as bar, commercial, museum, restaurant, church, hotel and office, which have been both associated with the building floor level when placed indoors.

Occupant loads have been defined as described in Section 3.1 and shown in the Supplementary Material S1. Regarding seasonal variations, two periods are considered: winter (from October to May) and summer (from July to September). In particular, higher risk levels are expected in summer periods due to the increase in *E* and *UV* factors. In fact, in summer, the population increases due to the arrivals of tourists, commercial activities widely operate into the night (i.e., bars and restaurants), also being hosted in dehors and outdoor areas, and most mass gatherings are organised.

For the purposes of this study, the following use and crowding scenarios are identified, by identifying the season and the operational conditions of mass gatherings (considering typical occupancy loads from Italian Fire Prevention Code [99]) and pedestrian areas (according to basic LOS [100]), being associated with different frequencies during the year:

- SC01: Winter, working day with low crowding conditions (No mass gatherings + pedestrian areas = 0.2 people/m^2, ideally referring to LOS A conditions): occurring 57% of the year;
- SC02: Winter, weekly market trade day (i.e., Thursday) and related crowding conditions (Mass gatherings areas = 1.2 people/m^2 from 6AM to 1PM + pedestrian areas = 0.2 people/m^2): occurring 10% of the year;
- SC03: Summer, working day with no event and low crowding values (No mass gatherings + pedestrian areas = 0.2 people/m^2): occurring 19% of the year;
- SC04: Summer, working day, with normal crowding values (Mass gatherings areas = 1.2 people/m^2 from 3PM to 12PM + pedestrian areas = 1.7 people/m^2, ideally referring to LOS F conditions): occurring 4% of the year;
- SC05: Summer, working day, with mass gathering events (Mass gatherings areas = 2.0 people/m^2 from 3PM to 12PM + pedestrian areas = 1.7 people/m^2): occurring 10% of the year.

To contemplate most recurring scenarios and the main levels of potential users' presences (from basic to critical), SC01, SC03 and SC05 are then selected for assessment purposes, in the given *PV* and *H* conditions as described in Section 3.4, and considering the five daily periods defined in Section 3.2, that are:

- NT = nighttime, from 1AM to 5AM;
- EM = early morning, from 6AM to 10AM;

[7] https://www.comune.senigallia.an.it/documento_pubblico/p-p-c-s-senigallia/(last access: 13.08.2025).

Fig. 7. Identification of the activities in the study area, considering residential (a), public (b) and mass gathering (c) intended uses.

- N = noon, from 11AM to 2PM;
- A = afternoon, from 3PM to 7PM;
- E = evening, from 8PM to 12PM.

In all these scenarios, demographic information about the city's population was collected from the Italian National Statistics website (ISTAT-2023 census database[8]) and divided into the five social categories, described in Section 3.2. Moreover, the percentage of unemployed adults in 2023 was set equal to about 8%, according to Italian national statistics.[9]

Finally, the following *PV* and *H* scenarios are considered in the case-study application:

- For flood, floodwater flows are considered perpendicular to the river axis (as in overflow) in view of the general configuration of the river in the case study area. The five *H* levels (negligible to extreme – see Section 3.3.2), and, thus, 5 *PVH* combinations have been assessed;
- For earthquake, all the return periods are considered in combination with scenario C3, to take into account the worst conditions on roof typology and effectiveness of seismic devices, which then could have higher impacts in terms of damage for the buildings and the facing open spaces. Other scenarios would be expected as less critical than the selected one, at each return period. Therefore, 4 *PVH* combinations have been assessed.

Finally, some additional details are provided to support the application of the methodology for earthquake *PVH* assessment. A uniform seismic hazard is assumed for all buildings: the municipality of Senigallia is entirely classified as seismic Zone2[10], and the historic centre analysed lies within a single homogeneous microzone according to the microzoning maps by the local Civil Protection.[11] No internal subdivisions or amplification hotspots are identified in maps, justifying the assumption of a spatially uniform PGA across the study area defined in Section 3.3.3. Moreover, buildings in the assessed UBE are traditional unreinforced masonry structures, which is the prevailing typology in the historic centre. The *Ivs* parameters implicitly capture the typical behaviour of masonry buildings, including lateral load-resisting characteristics, construction materials, and pre-code design levels. This justifies the use of the *Ivs* methodology for the entire building stock in its standard form, according to Section 3.3.3 methods.

5. Results

Results are represented by focusing on maps-over-time describing the different levels of risk of the open spaces for flood and earthquake scenarios selected in Section 4, providing them according to Section 3 outline, that is: users' exposure and vulnerability (Section 5.1); Physical Vulnerability and Hazard (Section 5.2); combination of *PVH* and Exposure, to represent the single risk-assessment and multi-risk comparison (Section 5.3). In particular, results are shown herein for SC03 and SC05, while SC01 is reported in Appendix A, being less critical in terms of users' presence. Moreover, all the values for the adopted indicators are reported in Supplementary Material S2, for these three scenarios.

5.1. Results on user exposure and vulnerability

Fig. 8 resumes the exposure *E* values in the case study area for SC03 and SC05, at the single open space level. Results are presented using the five-level representation scale (ranging from negligible to extreme exposure), and for the five daily periods defined in Section

[8] https://demo.istat.it/app/?l=it&a=2023&i=POS (last access: 13.08.2025).
[9] https://istat.it/it/archivio/occupati+e+disoccupati (last access: 09.12.2025).
[10] https://www.regione.marche.it/portals/0/Paesaggio_Territorio_Urbanistica/Sismica/Norme/DGR_1142_22/Allegato_A.pdf – in Italian (last access: 30.12.2025).
[11] https://www.protezionecivilesenigallia.it/piani-di-emergenza/rischio-sismico/- in Italian (last access: 30.12.2025).

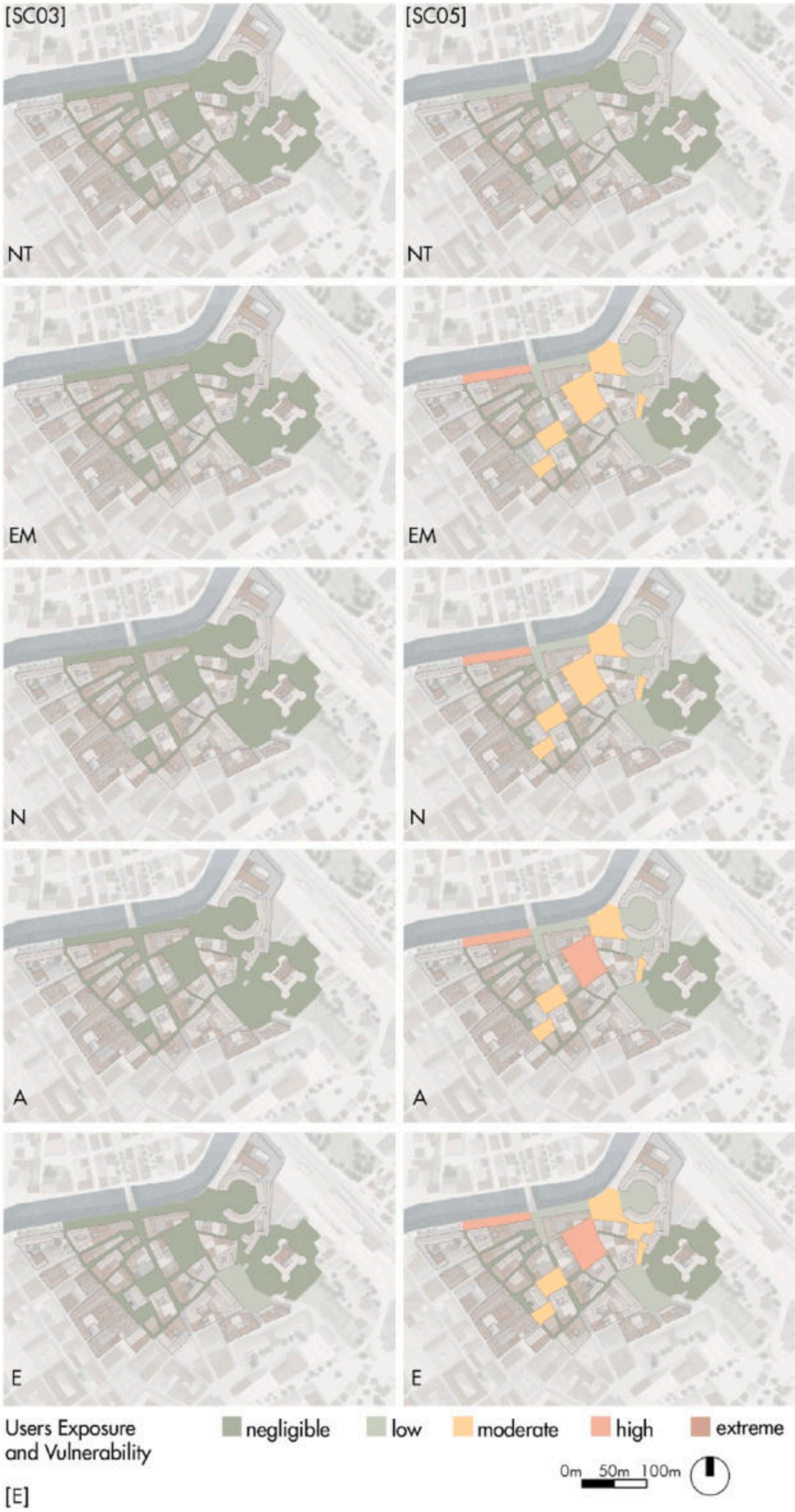

Fig. 8. Maps over time of *E* values at the open space scale: comparison between SC03 and SC05 for the considered five daytime periods (nighttime NT, early morning EM, noon N, afternoon A, evening E).

3.2. *E* is the same for flood and earthquake. SC03 shows limited temporal variability, with exposure levels ranging from negligible to low throughout the day. In contrast, SC05 exhibits significantly higher *E* values and a relevant variation between nighttime and daytime. This result is essentially due to: (a) the main presence of users in residential areas during nighttime, in both scenarios; (b) the limited crowding levels in SC03; (c) the relevant mass gathering conditions considered for SC05, which imply that the density of users during the day is more than three or four times the nighttime one; (d) the relevance of public activities such as bars and restaurants as users' attractors, increasing *E* especially in evening periods. As expected, higher *E* values are also associated with open spaces hosting public intended uses, as those of the main urban squares (see also the related markers in Fig. 7b).

As for the above, Figs. 9 and 10 show the users' vulnerability values related to age (*UVa*) and familiarity (*UVf*) issues, respectively, for SC03 and SC05. As for *E*, *UVa* and *UVf* are the same for flood and earthquake. Differences between SC03 and SC05 are based on the typology of hosted users, which is essentially affected by the opening times of public functions. Considering age issues (Fig. 9), differences between nighttime and daytime are generally slighter, especially for SC05, limiting *UVa* values up to moderate. Open spaces characterised by the highest *UVa* levels are essentially affected by the balance between vulnerable and non-vulnerable users according to Equation (2). In particular, four streets reach moderate *UVa* levels. With respect to the other open spaces, they are mainly characterised by residential uses rather than public activities, and thus the daily presence of vulnerable users (who are more likely to remain at home) increases. These streets could represent the effective "hot-spots" in emergency conditions, considering the vulnerable users' response and possible assistance needs.

Considering familiarity issues (Fig. 10), SC03 shows higher variability with respect to SC05, due to the higher importance of residents' presence. Nevertheless, the areas which mainly host public intended uses can be easily identified by those open spaces characterised by higher *UVf* values. These areas could represent hot-spots in emergency conditions: they can host a valuable quantity of users unaware of safety plans and procedures with respect to residents, possibly needing further assistance on where to go and how to behave. Furthermore, SC05 also graphically underlines how almost the whole historical UBE is an attractor of visitors during summer days and events, remarking the capabilities of the methodology in distinguishing between different use scenarios and related *UV* characterisation.

Finally, Fig. 11 compares users' vulnerability by position *UVp* considering disaster-specific characterisation of the indicators for flood (left side of Fig. 11, UVp_f) and earthquake (right side of Fig. 11, UVp_e). Fig. 11 underlines the capabilities of the methodology in identifying the main *UV* drivers in the given scenarios, and confirms general outcomes from previous works [21,22]. In particular, UVp_f seems to be generally higher than UVp_e, apart from the time period, in both SC03 and SC05. In fact, UVp_f considers users placed at the ground floor and outdoors, whose number is higher than that of users placed indoors at the upper levels, considering the predominance of ground floor activities and outdoor uses (compare with Fig. 8). These conditions are more relevant in SC05, where most people are visitors of mass gathering areas, thus being placed outdoors. In this sense, in SC05, *UVp* values seem to be quite homogeneous over time due to the long-lasting presence of these users over time. As expected, afternoon and evening periods seem to be the most critical ones, in view of opening times of public intended uses at the building ground floors, such as bars and restaurants, providing higher *UVp* values in both flood and earthquake since they are hosted indoors. Nevertheless, nighttime in earthquake conditions is more relevant than daytime periods, in view of the paramount role of residential uses.

5.2. Results on physical vulnerability and hazard

As expected, the proposed *PVH* assessment ensures tracing the increasing impact of the increase in *H* values, given the same *PV* conditions for each of the open spaces. Critical *PVH* threshold scenarios are then selected on these bases, considering the most critical ones in which users can generally activate emergency and evacuation procedures, for each of the analysed disasters.

In greater detail, Fig. 12 shows the *PVH* maps for flood (perpendicular to the river) under the five *H* levels (negligible to extreme – see Section 3.3.2). As expected, increasing *H* values implies that critical *PVH* values are first reached by open spaces placed along the riverside. A relevant *H* threshold could be represented by a moderate level, which could be assumed as the last one ensuring users' motion in a flooded scenario, since floodwater depths and speed conditions still allow pedestrian stability [49]. Under the moderate *H* scenario, Fig. 12 points out how the inner parts of the historical UBE seem to show limited *PVH* levels, as for the lower *H* levels. This scenario is then considered in the final risk comparisons (i.e., Section 5.3.3).

Fig. 13 shows the *PVH* maps for earthquake, considering C3 as *PV* condition and the four return periods defined in Section 3.3.3. When the return period is equal to or greater than 475 years, most of the open spaces are widely characterised by very heavy damage levels, especially considering the inner part of historical UBE. Nevertheless, although the high percentage of open spaces areas occupied by possible debris (mainly, non-structural ones), $H = 475$ years can still allow users to activate emergency response and evacuation process, and thus this scenario is then selected in the final risk comparisons (i.e., Section 5.3.3).

5.3. Final single-risk assessment and hot-spots identification

The final single-risk *R* maps of open spaces result from the combination of *E* and *UV* (Section 5.1) with *PVH* (Section 5.2), aggregated in the five time-periods. To demonstrate the proposed approach capabilities, according to Section 5.2, SC03 and SC05 are herein assessed at the open space level, in two different ways according to the research questions:

1. "How do different user factor conditions influence risk levels for the same SUOD?", in section 5.3.1. In particular, single risk maps are provided in the following, by occupancy load scenarios;

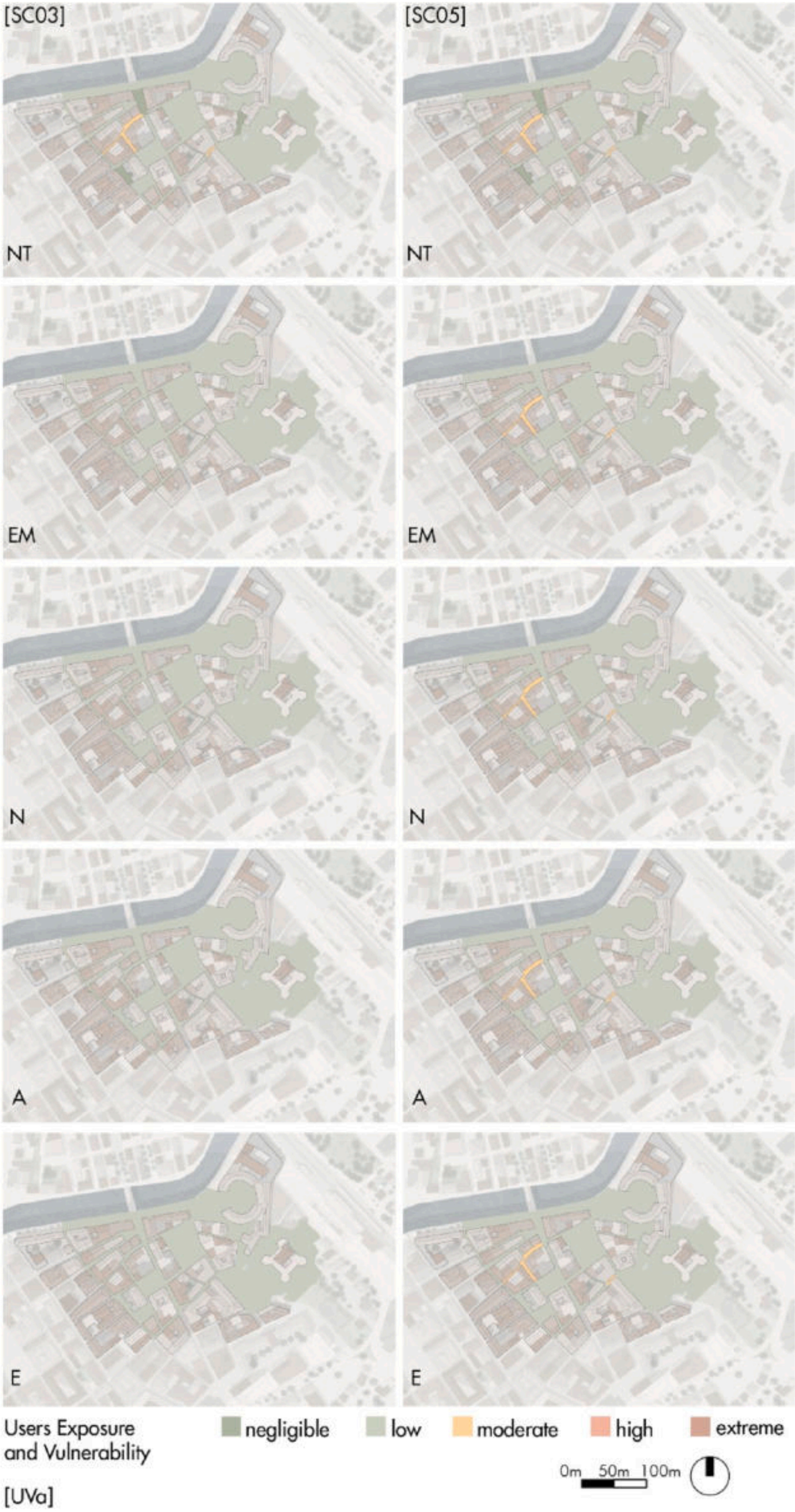

Fig. 9. Maps over time of *UVa* values at the open space scale: comparison between SC03 and SC05 for the considered five daytime periods (nighttime NT, early morning EM, noon N, afternoon A, evening E).

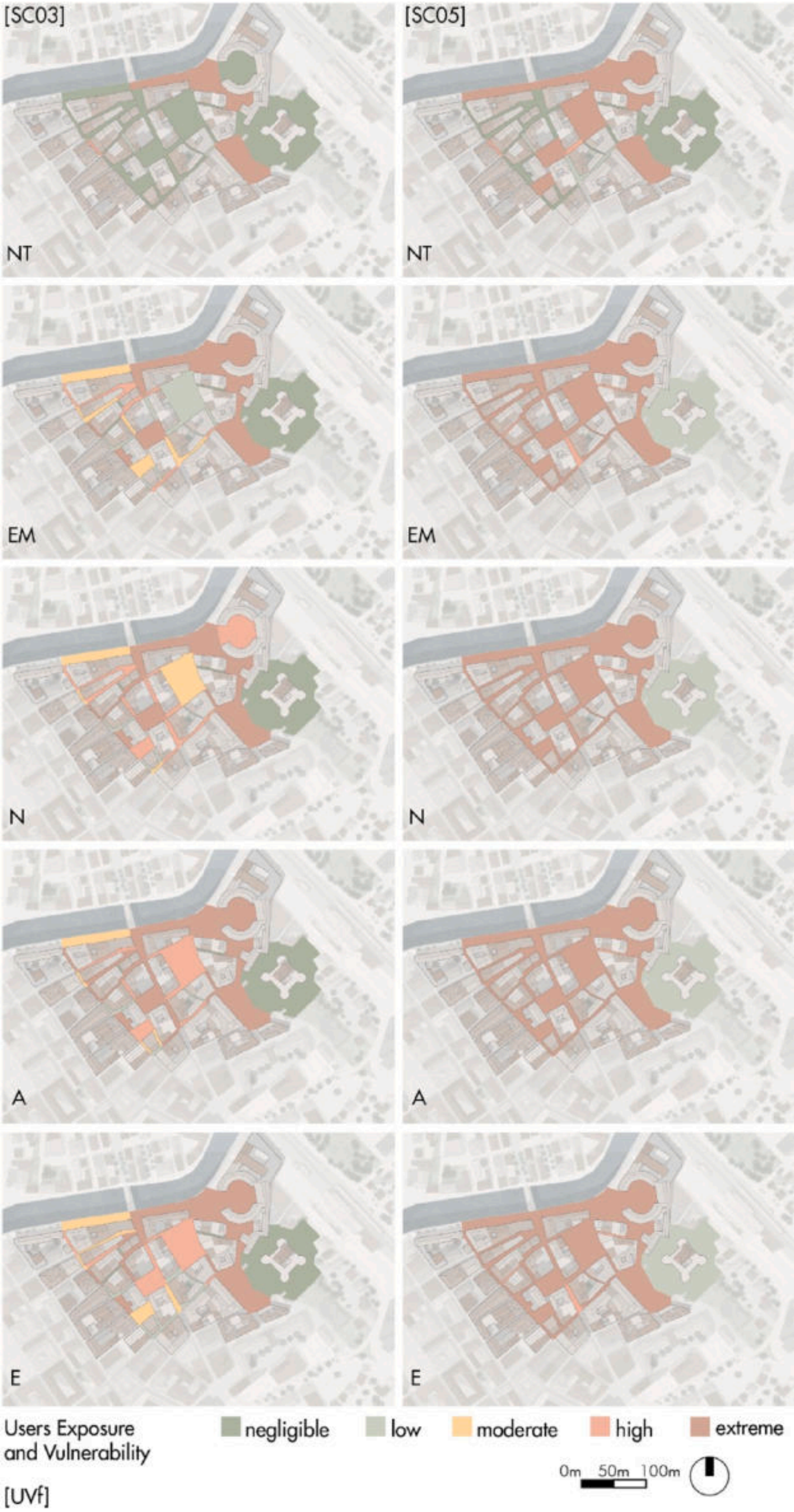

Fig. 10. Maps over time of *UVf* values at the open space scale: comparison between SC03 and SC05 for the considered five daytime periods (nighttime NT, early morning EM, noon N, afternoon A, evening E).

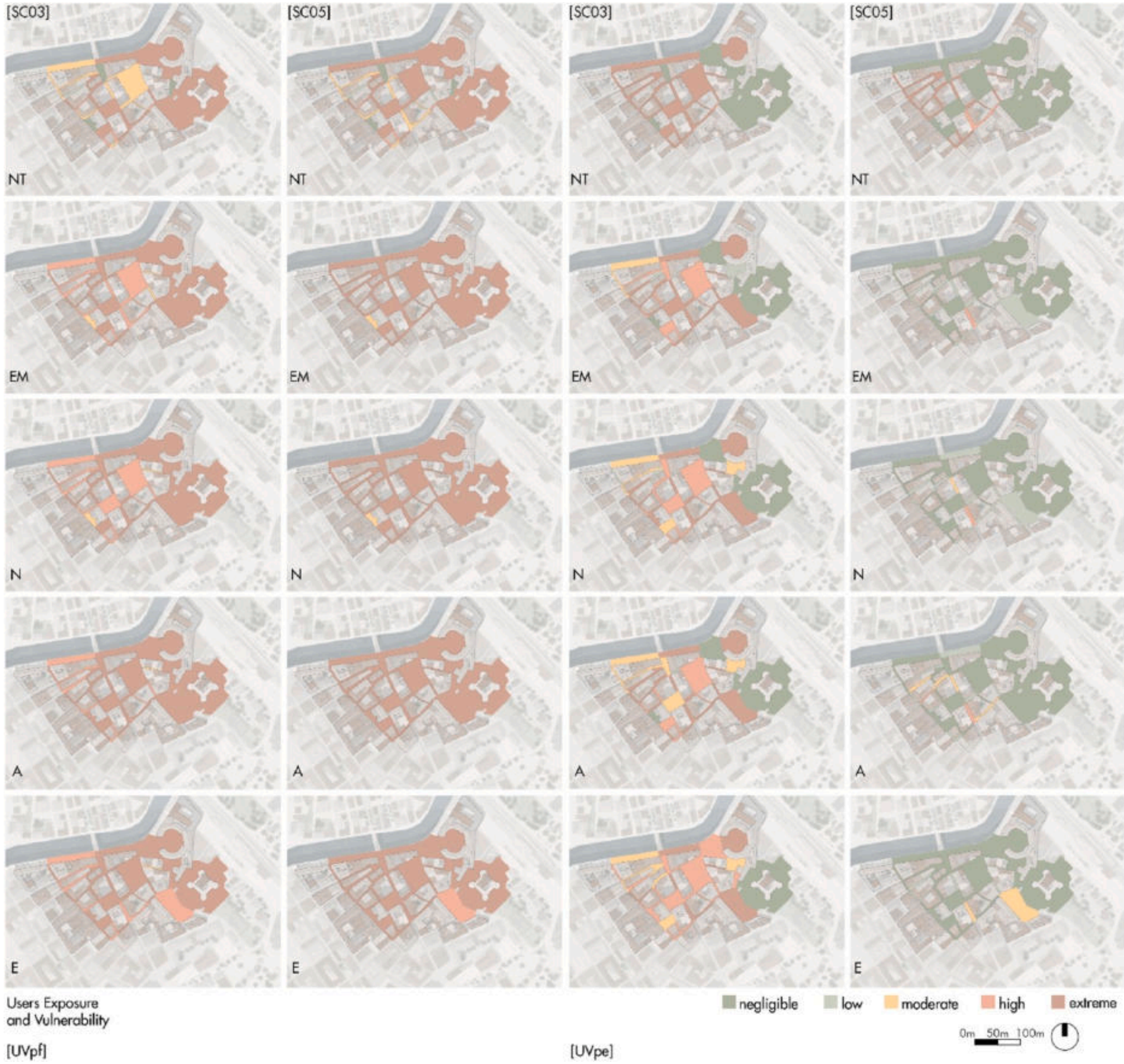

Fig. 11. Maps over time of UVp_f (left) and UVp_e (right) values at the open space scale: comparison between SC03 and SC05 for the considered five daytime periods (nighttime NT, early morning EM, noon N, afternoon A, evening E).

2. "How do different SUODs conditions affect the risk levels for the same user factor conditions?", considering the same SUOD under different *H* levels, in Section 5.3.2;

Moreover, as a combination of the previous questions, the direct comparison of flood and earthquake risk levels, under related scenarios that still ensure the activation of the emergency and evacuation process, is provided in Section 5.3.3, allowing to qualify multi-risk hot-spots depending on the most relevant disaster.

Nevertheless, other input conditions could be considered by applying the same methodology.

5.3.1. How do different user factor conditions influence risk levels for the same SUOD?

Figs. 14 and 15 show the final *R* maps, respectively in flood and earthquake scenarios, by comparing SC03 and SC05, under the considered *H* conditions, which still ensure the activation of emergency and evacuation procedures (respectively, i.e., moderate *H* levels, and return period of 475 years). Values are reported for each of the daily time periods.

Nighttime periods are the less risky ones, being affected by the limited presence of users, apart from areas generally involved in mass gatherings. This remark is mainly valid for flood scenarios, apart from the occupancy load conditions, while, in earthquake

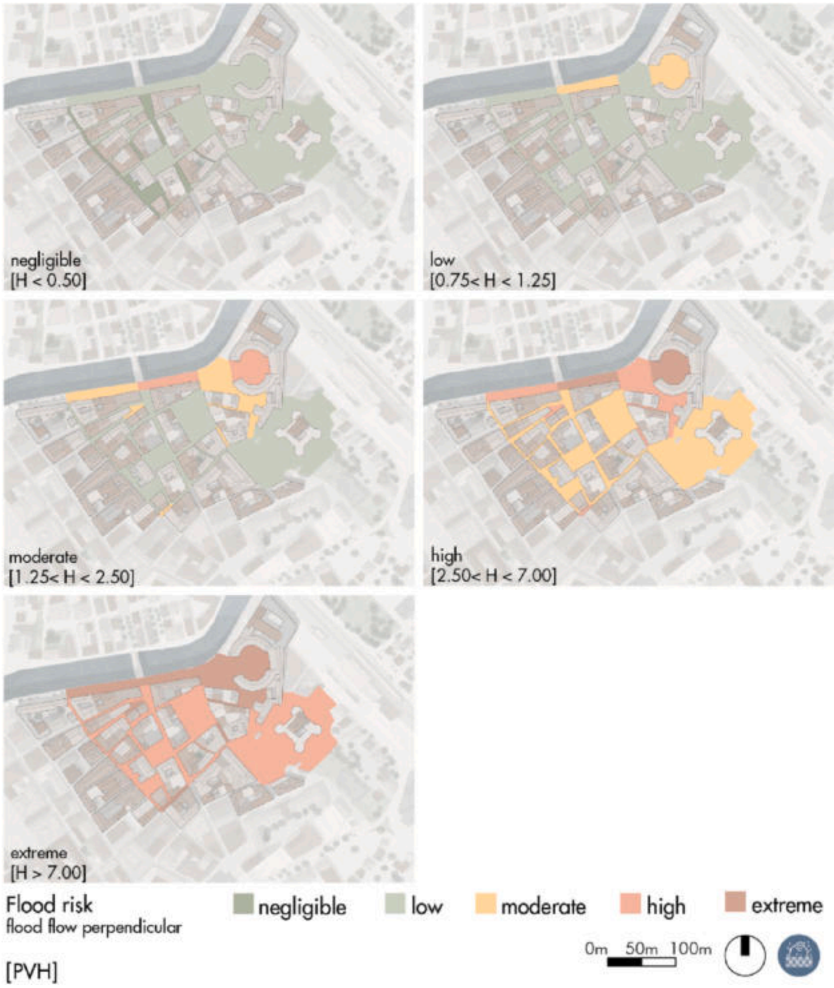

Fig. 12. *PVH* flood maps at the open space scale, for conditions of flood flow perpendicular to the river axis, under different *H* scenarios, as defined in Section 3.3.2.

nighttime scenario for SC03, risk levels are comparable to those of early morning and noon, in view of the influence of residential uses, confirming what discussed in Section 5.1. The other time periods show a more limited variability in *R* levels, essentially due to the relative variations of the risk factors discussed in Section 5.1. Additional differences in final *R* values in flood and earthquake scenarios are mainly due to the position of these users, depending on the *PVH* conditions. Nevertheless, as expected, afternoon and evening scenarios are the most critical ones. This is due to the combination of the increasing number of hosted users (*E*), mostly of them unfamiliar and unaware (*UVf*) and placed in risky locations (*UVp*), and the critical UBE conditions (*PVH*), which exacerbate final *R* levels. In fact, the higher the exposure and the more critical the users' vulnerabilities, the higher the risk given the same *PVH* conditions.

In this sense, from a general standpoint (that is, considering the historical UBE as a whole), it could be argued that flood scenarios seem to have a greater impact than earthquake ones, especially in SC05, essentially in view of UVp_f, which consider how most of users are placed at the ground floors (in bars/restaurants) and outdoors during mass gatherings. Conversely, SC03 maps demonstrate how more "normal" use conditions would imply higher risk levels for earthquakes, being mainly connected to the indoor functions.

5.3.2. How do different SUODs conditions affect the risk levels for the same user factor conditions?

Figs. 16 and 17 show the final *R* maps for SC05, respectively in flood and earthquake scenarios, depending on the considered *H* conditions (respectively, i.e., in terms of floodwater depth and speed, and in terms of return period). Values are reported for each of the daily time periods.

Considering flood risk (Fig. 16), *H*-related impact on *R* is more relevant during nighttime, due to the more limited (and less critical) *E* and *UV* values in this time period. Risk conditions during afternoon and evening timings seem to be similar in all the assessed scenarios, thus, regardless of the *H* conditions, being generally equal to moderate *R* levels. Moreover, for some hot-spots (i.e., open spaces along the riverside, main urban squares), high *R* levels can be noticed. In high and extreme *H* conditions, indeed, only a couple

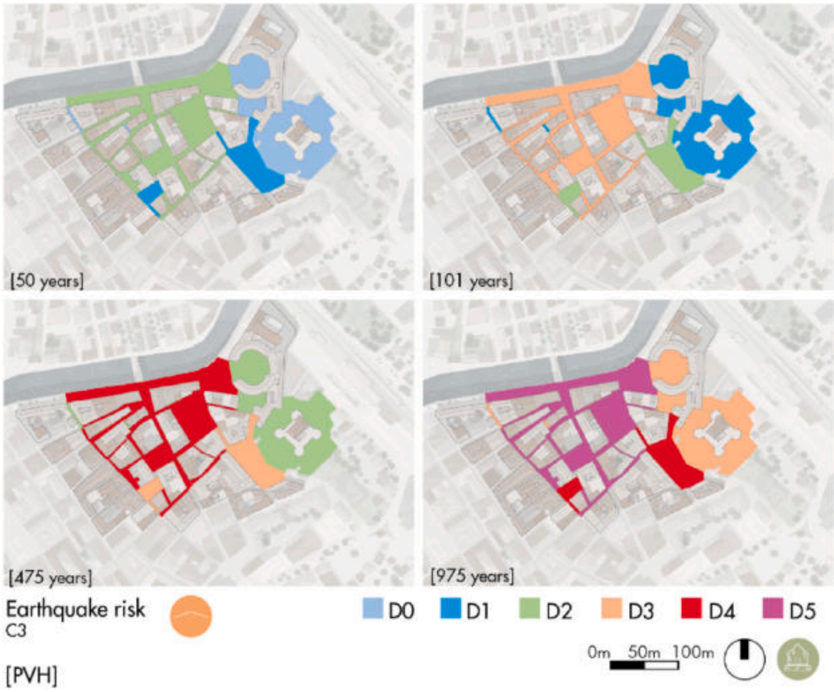

Fig. 13. *PVH* earthquake maps of PV scenario C3, at the open space scale, for each of the *H* levels defined in Section 3.3.3 in terms of return periods.

of open spaces, susceptible to mass gathering conditions, are added to these riskiest areas. As a result, it could be underlined that decision makers could select hot-spots identified in high/extreme *H* conditions to solve all the *H*-related scenarios.

Considering earthquake risk (Fig. 17), risk increases with the return period, as expected. 101 years and 475 years hot-spots are similarly identified in nighttime, early morning and noon occupancy conditions, while differences in afternoon and evening periods are limited to some main urban squares, mainly in view of the attraction of users in their buildings. In 975 years-related scenarios, *R* values are similar apart from the time period, remarking how damage conditions correlated to *PVH* maps seem to be more relevant for earthquake risk assessment than the use dynamics, as expected.

5.3.3. Multi-risk comparison

The Risk Ratio *RR* (Section 3.4.2) is applied to SC03 and SC05, for all the time periods, considering moderate *H* levels for flood and a return period of 475 years for earthquake (as explained in Section 5.3.1). Fig. 18 provides the related results, marking *RR* values lower than 1 in red (predominance of earthquake risk) and higher than 1 in blue (predominance of flood risk). As an output, Fig. 18 graphically traces the open spaces that are, respectively, hot-spots, especially for earthquake and flood scenarios. This can support decision-makers on where to focus efforts to solve related issues and promote disaster-specific strategies. Related numerical values of *RR* are reported in Appendix B.

In SC03, Fig. 18 shows how the distribution of *RR* values reveals that disaster conditions due to earthquake seem to be more relevant than those referring to flood, although a relatively balanced interplay between the two disasters can be noticed. In fact, *RR* generally ranges from 0.4 to 1.4. Indeed, flood risk tends to dominate in focused hot-spots located near riverbanks, especially when public intended uses are present. These conditions can be mainly noticed in the nighttime scenario for SC03, due to the poor presence of residential uses in these open spaces. On the contrary, in the same nighttime scenario, earthquake risk is higher than in daytime periods due to the higher presence of residents among the users.

Conversely, SC05, which relies on higher user presence, presents a more marked spatial differentiation, with a more relevant impact of flood risk. In fact, *RR* ranges from 0.6 to 2, being unbalanced towards critical expected flood risk conditions. In particular, flood risk becomes clearly predominant in open spaces adjacent to the river and in several large public squares, as indicated by *RR* values consistently greater than one. These areas are mainly populated by users placed on the ground floors and outdoors, making them highly exposed to flood scenarios. In contrast, the historic core, especially those streets characterised by dense building and higher *PVH* values, but more limited users' exposure and vulnerability, shows $RR < 1$, indicating that earthquake risk remains the primary concern in these zones. Moreover, as for SC03, the analysis of SC05 still remarks the predominant role of earthquake risk during nighttime, as expected in view of the effects of residential uses [21,22].

6. Discussions and final remarks

Assessing risk in flood and earthquake emergencies can take advantage of a spatiotemporal characterisation of both user-related

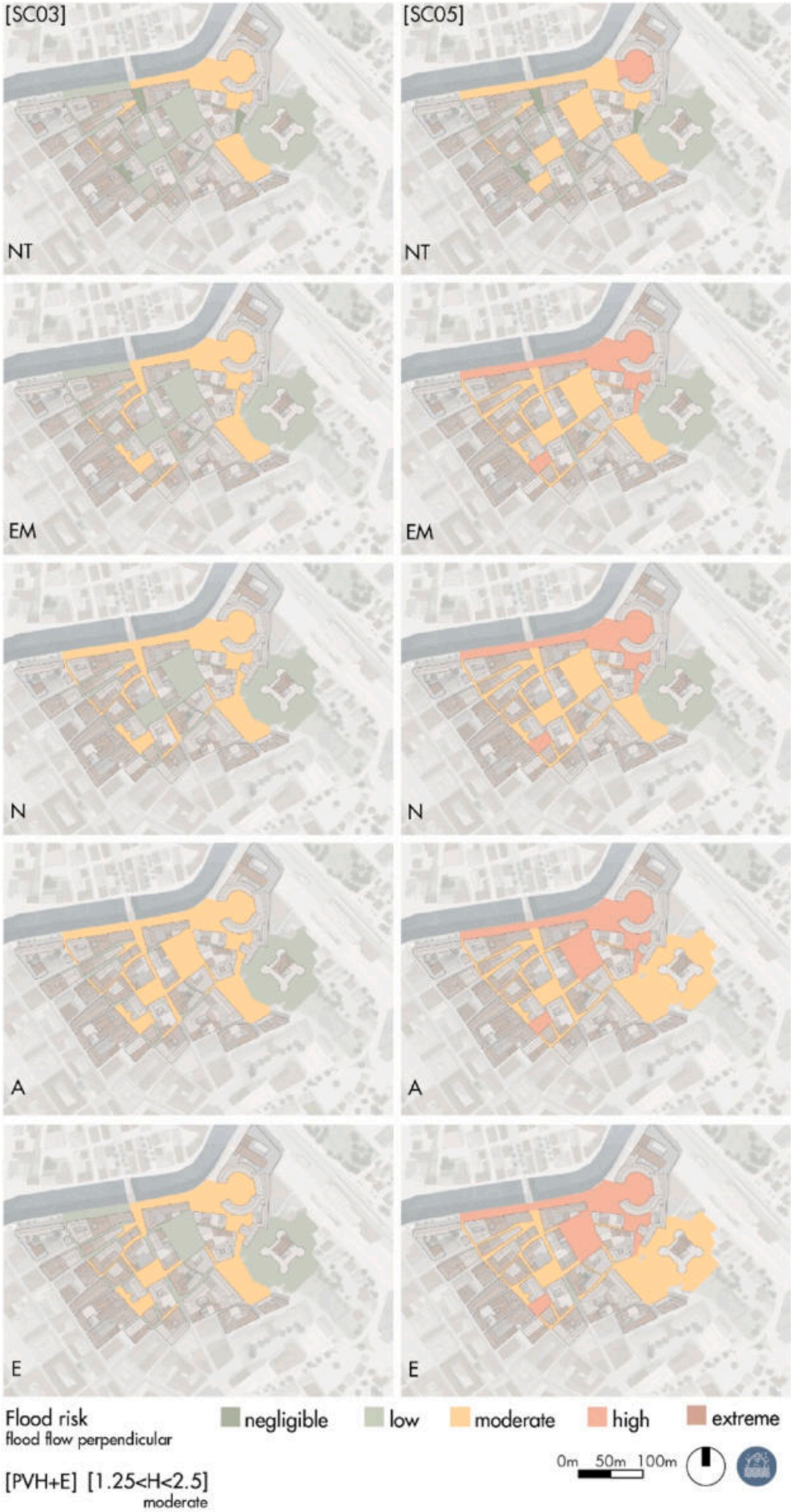

Fig. 14. Maps over time of single risk for flood at the open space scale: comparison between SC03 and SC05 in moderate *H* scenarios allowing the activation of emergency and evacuation procedures.

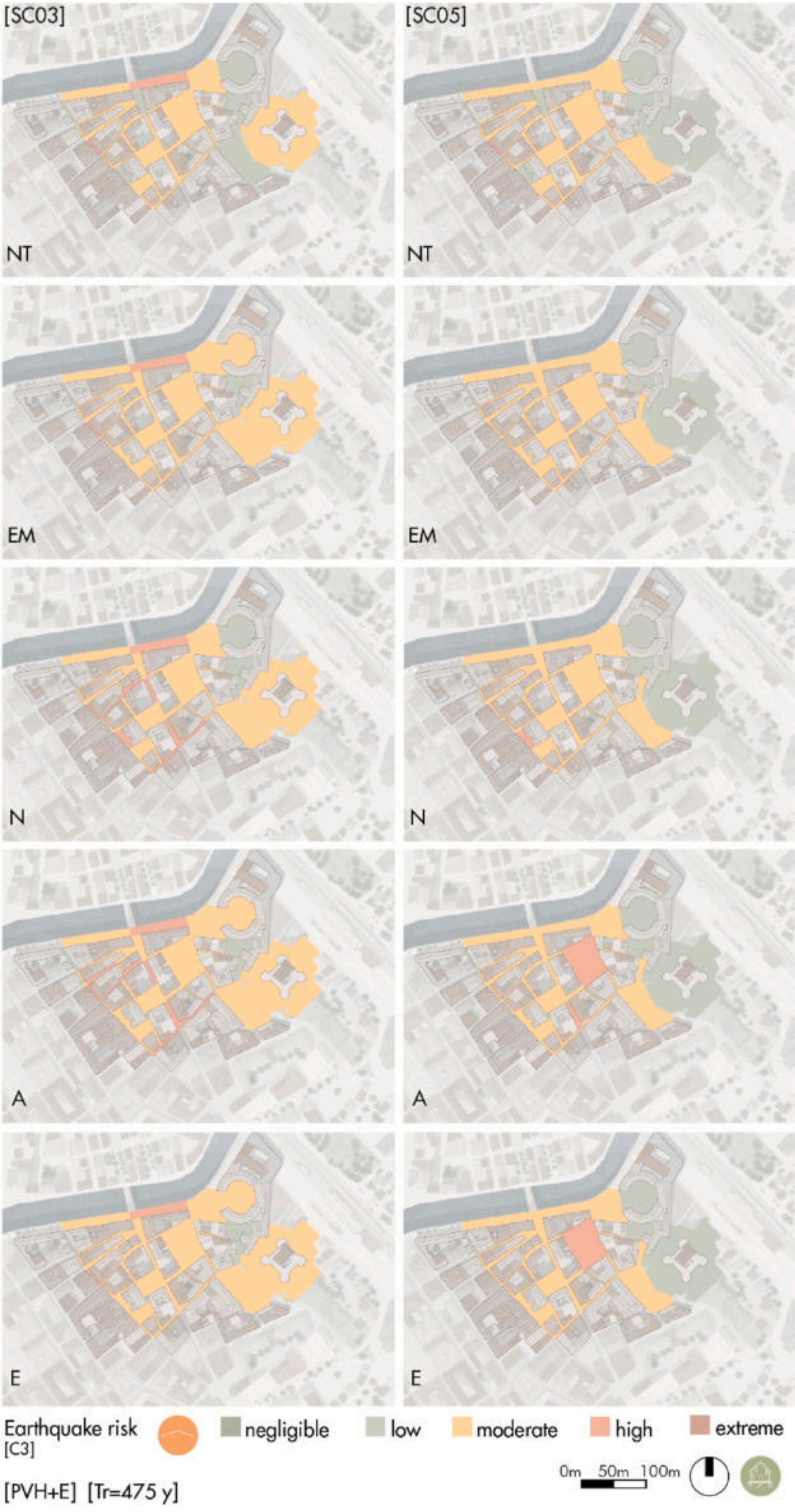

Fig. 15. Maps over time of single risk for earthquake at the open space scale: comparison between SC03 and SC05 in scenarios (C3, $H = 475$ years) allowing the activation of emergency and evacuation procedures.

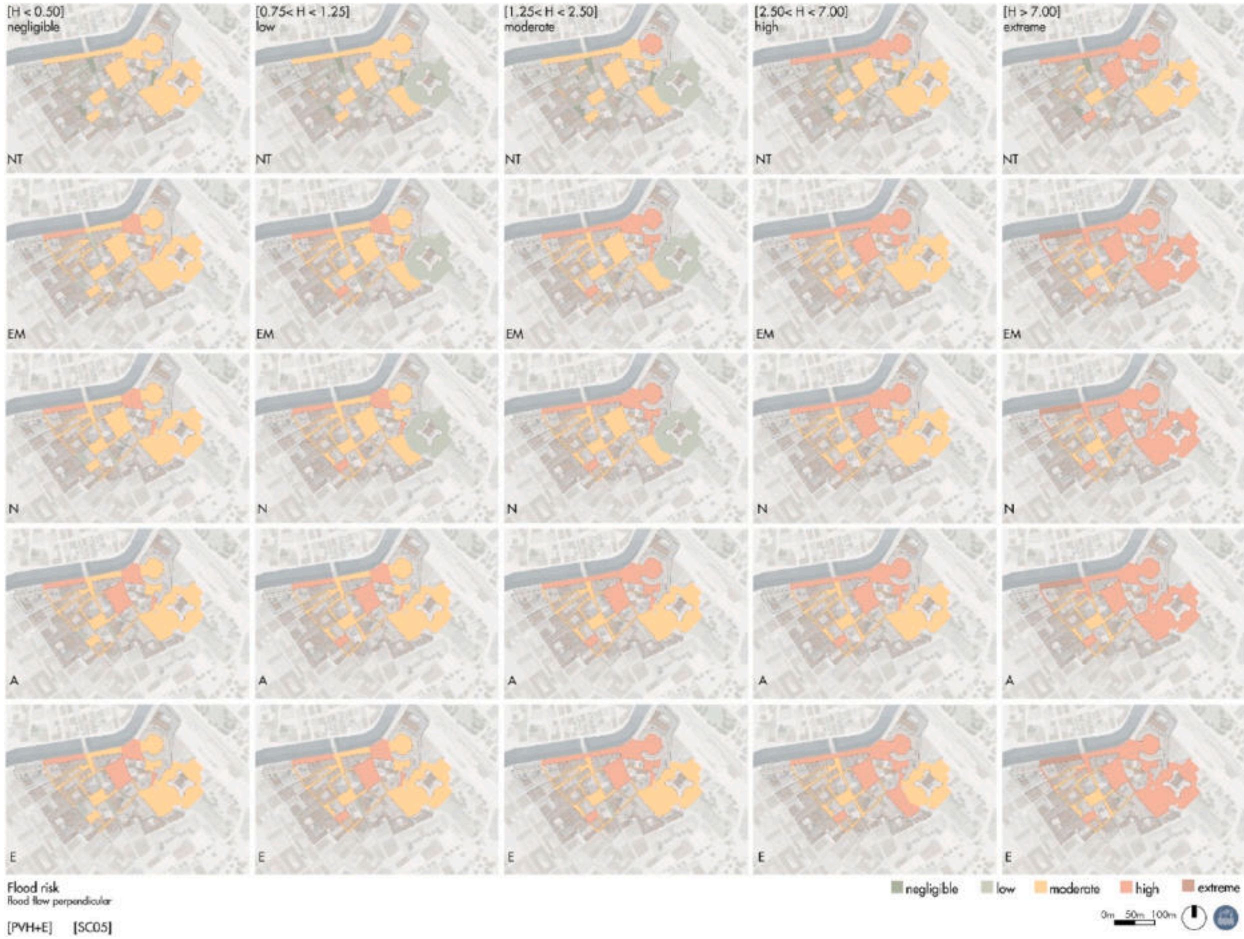

Fig. 16. Maps over time of single risk for flood at the open space scale: comparison between different *H* levels for water flows perpendicular to the river, under time periods for SC05 as occupancy scenario.

factors and physical features of the built environment, differentiated across hazard scenarios. This work proposes a rapid methodology to compare multiple scenarios through a multi-layer single-risk approach applied at the mesoscale, that is considering open spaces as critical for user dynamics and emergency response. By adapting validated building-level methods to the mesoscale deployment, the approach overcomes the limits of traditional assessments based on static or point-based analyses. In particular, it addresses a "dynamic" perspective in risk assessment thanks to the developed time-dependent framework, which allows the explicit spatiotemporal evolution of exposure and vulnerability (based on an hourly-based representation scale, for each analysed open space). This allows for a more comprehensive risk evaluation.

The proposed methodology effectively meets the research objectives defined in Section 1, by enabling both single- and multi-risk comparisons: (1) across different hazard types under consistent spatiotemporal use conditions, and (2) across varying user dynamics under constant hazard scenarios. This dual comparison framework enhances the granularity and operational relevance of urban risk assessments, providing insights into how user presence patterns influence exposure and vulnerability across different risk contexts.

The application of the methodological workflow to a representative historical UBE confirms its feasibility and practical relevance, supports decision-making processes (Section 6.1), and highlights both current limitations and directions for future research (Section 6.2).

6.1. Key findings and implications for the approach application

The application of the methodology to the historical UBE of Senigallia (Italy) demonstrates its capacity to identify scenario-sensitive hot spots for earthquake and flood risk by integrating physical vulnerability with the spatial and temporal dynamics of users. The following key findings from the case study emerge:

a. While overall criticality levels are comparable for earthquakes and floods, their spatial distributions diverge significantly. Flood risk concentrates in open spaces near the river, where hazard intensity and user exposure converge. These areas are the widest

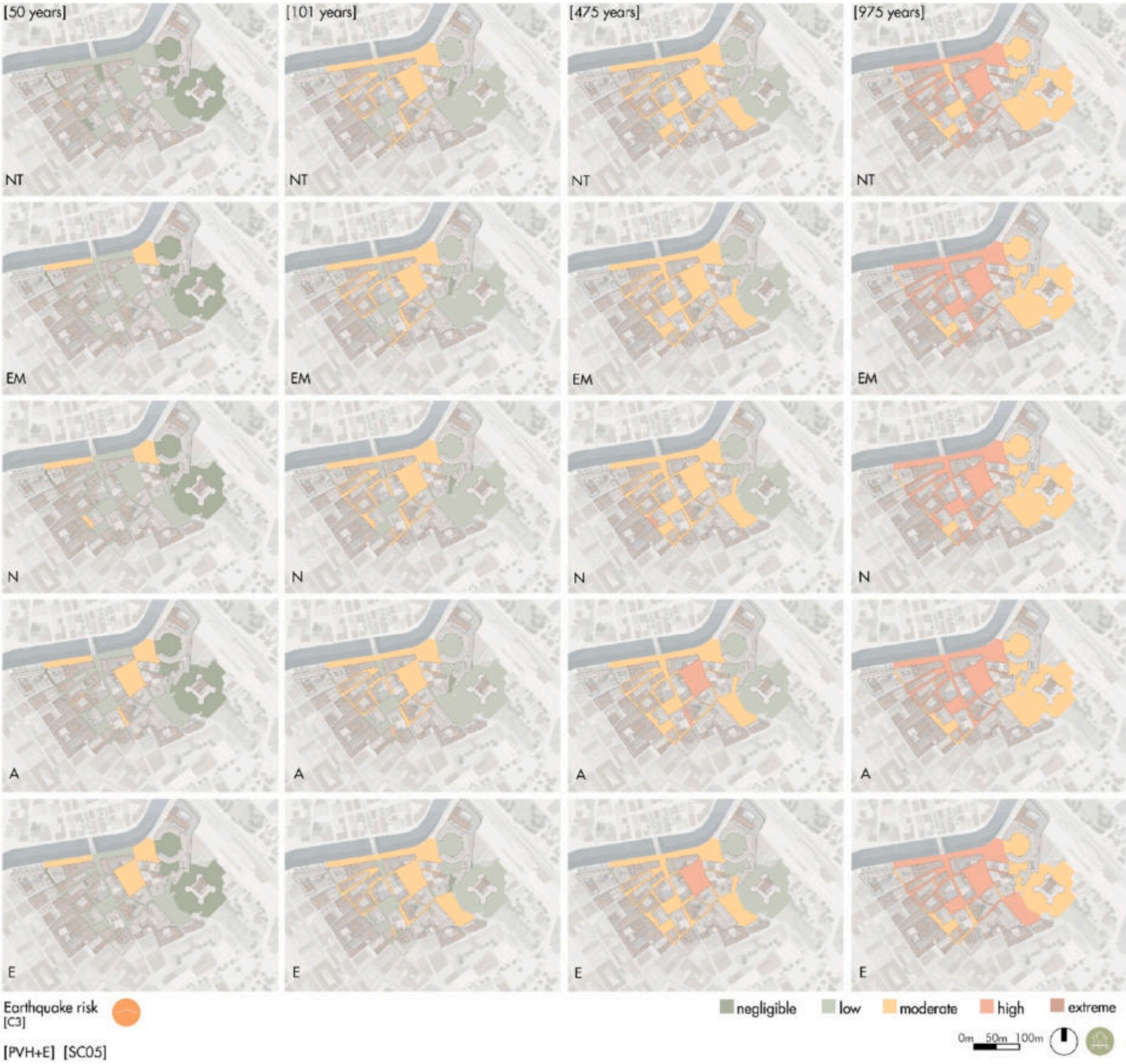

Fig. 17. Maps over time of single risk for earthquake at the open space scale: comparison between different *H* levels for *PV* condition C3, under time periods for SC05 as occupancy scenario.

streets and squares, hosting many users on ground floors or outdoors, especially during mass gatherings. Earthquake risk hot spots, instead, occur along the internal street network, where high building density and pedestrian circulation increase exposure and vulnerability;

b. The distinction provided by point (a) emphasises the importance of hazard-specific mapping to support targeted mitigation. The combination of strategies oriented towards flood risk awareness (including alerts and evacuation activation) and mitigation (e.g., structural solutions like flood barriers) would be beneficial for the open spaces placed along the river. Physical interventions on building seismic vulnerability would be more effective for the inner parts of the UBE. At the same time, deeper vulnerability assessment actions could be proposed in the same areas, to reach a more detailed analysis of seismic effects. This can guide decision makers in the allocation of related resources;
c. Differences in occupancy scenarios imply differences in risk levels for both the assessed disasters. Nevertheless, impacts also depend on the specific single risk. In fact, conditions typical of days with mass gatherings (SC05) are affected by the most critical risk effects, as expected. However, in this context, the high concentration of people in exposed open spaces, particularly in urban squares as public attractors, leads to increased risk levels, as flood scenarios pose greater threats to outdoor users. Conversely, for earthquake risk, typical winter days and summer days without public events (i.e., SC03) are affected by more severe risk levels, due to the assumption of predominantly indoor user presence. This is due to the expected higher number of people staying indoors,

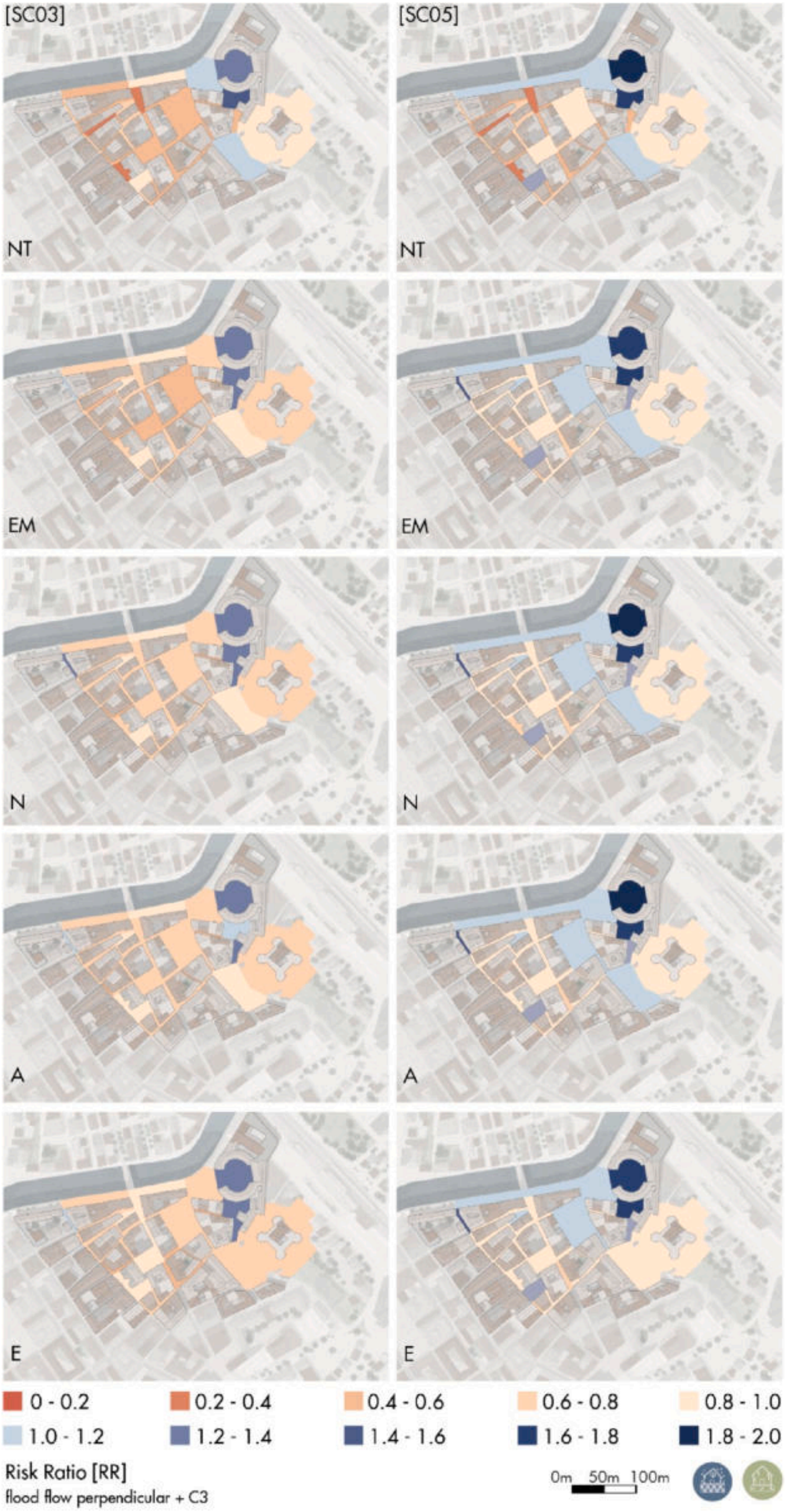

Fig. 18. Maps over time of Risk Ratio *RR* comparison: SC03 and SC05 (Perpendicular water flow, moderate flood hazard; return time of 475 years in C3 conditions of *PV*).

where vulnerability to structural collapse is significantly greater in the event of an earthquake. Such scenarios mainly refer to residential buildings, especially during the night, and to indoor public facilities, especially during the afternoon;

d. The spatiotemporal comparisons between flood and earthquake risk maps (through the Risk Ratio *RR*) under the considered occupancy scenarios stress how the use dynamics alter the predominance of the more relevant disaster in the assessed historical UBE. These results confirm point (c) findings, leading the decision-makers to rapidly identify the most critical disaster-specific hot-spots already traced by point (a);
e. Finally, findings from points (c) and (d) underscore the necessity of integrating temporal and seasonal variations into risk assessments, useful to adopt a spatiotemporal approach to the design, deployment and adaptation of risk reduction and mitigation strategies defined at point (b). Structural interventions to mitigate seismic vulnerability of building heritage would be beneficial in all the scenarios (mainly, during the majority of the year, since SC01 and SC03 represent more than 60% of the year days). Conversely, risk alerts and emergency planning in flood conditions should be more detailed for the touristic season (as in SC05). This also implies balancing the efforts of management planning and non-structural strategies, such as rescuers' deployment, to increase response capabilities in case of critical occupancy loads. These reasonable results, which are commonly borne in mind by decision makers, are quantitatively supported in terms of risk impacts by the maps provided in this work methodology, boosting the identification of hot-spots among the public open spaces.

In view of the above, the streamlined yet adaptable nature of the methodology underscores its transferability to other UBEs. While the current application focuses on Senigallia, the framework can be readily applied to diverse urban contexts, supporting integrated risk governance approaches that are both scalable and responsive to local specificities from the standpoint of decision-makers’ needs.

On the one hand, the key strength of the proposed approach relies on its ability to incorporate user-centric variables into risk mapping at the urban scale, which proved essential for interpreting how temporal fluctuations in users' distribution affect the severity and localisation of risk [14,21–23,41]. The open-space-centred perspective, combined with the flexibility of scenario-based modelling, can significantly support the integration of additional, consistent indicators to existing frameworks focused on a spatiotemporal perspective of risk levels [16,29]. The multiscale (micro-to-meso) structure of the assessment allows the aggregation of building-level data to the operational scale at which many emergency decisions are made (urban streets, squares and mass gathering areas). Such outputs are aligned with real-world decision-making contexts [4,41,43,57,58]. In addition, the methodology's ability to incorporate typical occupancy schedules, both considering the quantity and quality of the users, can provide a reliable basis for the definition of alternative “what-if” scenarios, which can then also be assessed using additional quick methodologies at both the building and open space scale. For instance, the users' typology and presence can be overlapped with the intended use characterisation and with the physical vulnerability analysis, so as to estimate dynamics in expected losses, including casualties or economic losses, using and thus enriching the contents and outputs of other established methodologies [22,29,91].

In this context, it is worth noting that the proposed workflow can move towards some relevant improvements over the state of the art. First, the adoption of hourly-based analysis on the user presence aligns with recent advances in dynamic population modelling [21,27,41], but this work represents an improvement by framing temporal variability within a hazard-agnostic structure, suitable for application to diverse risks and especially to complex historical UBEs [47]. The authors would clarify that, unlike previous studies [21], the proposed framework does not model dynamic exposure and vulnerability through direct variations in population density. In fact, according to consolidated approaches [25,41], population densities are derived from the application of occupancy schedules and standardised occupancy loads from fire safety regulations. Instead, dynamism is captured through a multi-scenario representation of user presence, built upon the intended use of spaces and their presence temporalities (e.g., by opening times for public buildings, and by typical home use schedules). Exposure and vulnerability vary according to hourly, daily and seasonal shifts in functional occupancy, rather than through density measurements, therefore offering a structure that is transferable across hazards and applicable also where high-frequency population data are unavailable. Second, previous reference work for the characterisation of user factors focuses exclusively on floods and on a single-risk framework. [41]. Conversely, this work extends the dynamic exposure–vulnerability methodology to a multi-risk context, adapting and recalibrating parameters so that the same mesoscale logic can be consistently applied to both floods and earthquakes. Third, recent applications of the single-risk multi-layer approach, such as in regional-scale studies [15], operate at a broad territorial scale using aggregated information. By contrast, the present work applies the same conceptual framework at a meso-scale, enabling a more detailed representation of the built environment, users, and hazard interactions within a historical UBE. This finer resolution allows the methodology to capture localised spatial dynamics and facilitates its operational use for urban-scale decision-making.

On the other hand, the workflow outputs can provide a more nuanced emergency management planning, offering a basis for dynamic, context-specific risk-reduction mitigation strategies, also providing a quantitative and easy-to-apply basis for their localisation through the hot-spot-based analysis [29,87,112]. This action can pave the way toward proper, informed decision-making support in UBEs [2,85], especially for emergencies where rapid access to localised and scenario-specific risk information can significantly improve the efficiency of resource allocation and intervention prioritisation. In particular, the proposed approach can hence contribute to the implementation of dynamic people-centred assessments in the operationalisation of BBB principles within the preparedness phase, in line with the Sendai Framework priorities on understanding disaster risk and investing in risk reduction [7,31–33,61]. The methodology for scenario creation can be evaluated by combining alternatives in preparedness and awareness strategies (mainly acting, e.g., on *UVf*), UBE uses (affecting *E* and *UV*) and physical interventions on buildings and open spaces (impacting *PVH*), according to the aforementioned key findings list. Finally, the operational workflow could also be extended to other kinds of SUODs affecting UBEs and other large urban areas, such as wildfires and landslides.

6.2. Limitations and future works

While the proposed methodology demonstrates significant potential, some limitations must be acknowledged, which also indicate directions for future developments.

First, the data collection on the use patterns of buildings has been conducted manually through the analysis of available documentation about building use and occupancy. This procedure is time- and resource-intensive, and it may limit applicability in larger or data-scarce urban areas [56,88]. Nevertheless, different techniques and databases could be implemented in the workflow without altering its basic structure, to facilitate more rapid and comprehensive data collection and organisation. Concerning user factors, this work adopts standardised occupancy loads from fire safety regulations for the creation of critical (but theoretical) scenarios. Nevertheless, the workflow could be updated using density-based variations [21], overcoming the simple association between standardised loads and typical use schedules. Moreover, taking into account previous approaches [42,54], additional integrations could rely on: (a) the use of databases on public intended uses, thanks to integration between BIM-GIS integration (e.g., net areas); (b) the use of point-of-interest data or online presence estimation tools (e.g., using Google Maps to get information about busy areas and activities[12]). These steps will move towards more effective and sensitive scenario creation on user presence and typologies. Concerning building vulnerability, this work estimated basic parameters using quick, standardised methods (i.e., relating to anti-seismic devices), and could be refined with further in-situ surveys or detailed structural assessments [105]. The manual collection of data represents, also, a limit for real-time data sources, such as seismic and hydrometric sensors, real-time crowd data, or dynamic GIS platforms [42,82]. Thus, embedding real-time monitoring could update risk outputs continuously, enhancing operational value for both preparedness and emergency response. The authors would acknowledge that all these data collection techniques (and, in particular, survey-related tasks) can be very time- and resource-consuming. However, they could improve the reliability of outputs, and they may therefore be used to enhance the quality of results after a general rapid assessment. In this sense, they could also be focused and tailored towards the main criticalities which emerged from the rapid methodology application. The proposed indicators would just be arranged depending on these outcomes, and, thus, without methodological changes in the criteria and workflow steps.

Second, indicators for risk assessment consider the conditions of the UBE before the event, and the severity of the disaster, but do not include results from emergency simulations. Hence, future steps should include the integration of simulation-based assessment, comprising floodwater spreading, earthquake debris, and evacuation simulation [24,49,85,86]. This integration would allow a more accurate, scenario-specific assessment depending on the number and typology of exposed users. It would also provide actionable insights for emergency planning, crowd management, sheltering deployment, user relocation and behavioural response to warnings. In this context, combining indoor/outdoor user distributions would allow estimating the number of individuals moving into and occupying each open space under specific emergency scenarios, as well as the identification of potential bottlenecks. Overall, the integration of such dynamic evacuation modelling would complement the current index-based approach through a more detailed representation of risk dynamics while preserving meso-scale applicability.

Third, the aggregation structure adopted for the risk metric could present a potential assessment limitation for decision-makers. The overall risk score is obtained through a weighted linear aggregation of normalised indices. This approach ensures transparency, interpretability, and an easy comparison across scenarios, being consistent with the decision-oriented objectives of the study [75,109]. Nevertheless, it does not explicitly model non-linear interactions among risk components, including potential threshold effects, feedback mechanisms, or compounding behaviours between hazard intensity, physical vulnerability, and user-related factors. The proposed framework and the use of comparison indices also support preparedness planning and scenario comparison at the urban open-space scale, rather than statistical prediction, providing clear prioritisation cues for decision-makers across multiple hazards, time slots, and use conditions. Furthermore, the use of Artificial Intelligence techniques, such as Machine Learning, could boost the process, by also allowing to screen risk factors which are not currently included in the proposed methodology [113–116].

Closely related to the aggregation structure, it is also important to acknowledge how modelling assumptions may influence the resulting risk patterns and their interpretation for decision-making purposes [75,109]. On the one hand, the indicators adopted for hazard, physical vulnerability, user exposure and user vulnerability are derived from validated methodologies [25,41,44–46,59,105], but their parametrisation may still influence the relative risk rankings across open spaces. Assumptions related to occupancy levels, temporal distribution of users, and the weighting structure of the risk components can also affect the magnitude and spatial pattern of the resulting risk indices. On the other hand, the weighting rules of risk components should also be further explored. A formal sensitivity analysis is not included in the present study, due to the above reliability remarks, and considering that this preliminary work contributes to the capability demonstration of the proposed methodology. While the current implementation prioritises transparency and operational applicability, future developments should include formal sensitivity and uncertainty analyses to systematically evaluate the influence of individual parameters and weights on the final outcomes. Such analyses could explore variations in AHP–derived weights, alternative normalisation schemes, or different assumptions regarding user presence and behaviour across time slots, thereby providing quantitative insights into the robustness of the proposed rankings. Incorporating sensitivity analysis would also support the adaptation of the workflow to different urban contexts, hazard conditions, or decision-making priorities, helping decision-makers understand which factors most strongly drive risk levels and where targeted data refinement efforts would yield the greatest improvements in reliability.

Fourth, within the modelling assumptions, the current approach provides two different minimum *PVH* class values, equal to 0.2, for

[12] E.g. see https://support.google.com/business/answer/6263531?hl=en&sjid=14839815015492539827-EU (last access: 25.08.2025).

flood, and to 0 for earthquake, respectively associated with the negligible class and the D0 class in the damage matrices. The conceptual meanings of this minimum condition in *PVH* and its effects on the facing open spaces are different:

- For earthquakes, D0 truly denotes absence of building damage (hence $PVH = 0$), which does not contribute debris or building-related adverse effects to the open space;
- For floods, the practical focus of the adopted flood matrix is on the effects that even small inundation conditions (shallow water/low speed) have on open space functionality and user safety; therefore, the flood matrix was calibrated so its lowest category corresponds to a small but non-zero operational effect.

Under this logic, the “negligible” flood condition can coherently encompass both the D0 and D1 seismic classes. This alignment does not affect the present study but offers a structured pathway for future refinements aimed at ensuring full cross-hazard consistency. In particular, a more harmonised treatment of the lowest hazard classes could be achieved by introducing an explicit “dry/no-impact” flood condition ($FHI = 0$), which would correspond to a *PVH* equal to the theoretical “zero”. Such a condition would be suitable for preventive emergency and evacuation scenarios, e.g., when users receive early warning and are requested to respond before the flood event strikes the given open space [117]. This adjustment could be mainly provided by modifying the flood matrix to include a “zero”-hazard class. Such an update would make the two *PVH* scales more directly comparable and would enhance the interpretability of both the maps and the resulting Risk Ratio, without altering the conceptual structure of the method. At the same time, given the need for sensitivity analysis [75,109], future works could also systematically evaluate how alternative *PVH* scores may influence the prioritisation of open spaces. This approach would entail conducting scenario-based sensitivity tests in which, for example, “negligible” is mapped to 0.0 instead of 0.2. Such an analysis would provide a robust understanding of the consequences of adopting more or less conservative assumptions in practical applications.

Fifth, the proposed framework focuses on users located in open spaces and incorporates the effects of building damage [46], but it does not explicitly account for user exposure associated with transportation networks and mobility infrastructures (e.g., bridges, roads, or public transit). This limitation is mainly relevant for the earthquake risk. Similarly, other typologies of infrastructures, including drainage systems and blue-green infrastructures, are not included in the current study, considering, for instance, their impacts on *PVH*. This limitation, indeed, can be mainly relevant for the flood risk. Future works should address this limitation by integrating infrastructure vulnerability and its consequences for users and UBEs [14,24,57,97]. This can enhance the comprehensiveness of the assessment, particularly in densely populated urban areas, and support a more complete multi-hazard risk evaluation that complements the current building- and open-space-centred approach.

Sixth, the absence of explicit loss assessment criteria can restrict the analysis to the comparison of relative risk levels without quantifying potential consequences in terms of physical damage, economic loss, or social impacts [22,29]. Incorporating loss estimation, particularly those accounting for different user categories and their specific vulnerabilities, would enhance the decision-making value of the methodology, enabling more precise prioritisation of interventions and resources [52,53]. Indeed, the proposed definition of use scenarios could support the analysis in alternative “what-if” scenarios. In this perspective, future extensions could also explore alternative aggregation schemes, including non-linear formulations or probabilistic combinations of risk components (e.g., based on fragility curves or damage matrices), as well as formal sensitivity and uncertainty analyses to assess the influence of weighting assumptions, as discussed above.

Despite these limitations, the proposed methodological framework provides a robust foundation for advancing integrated approaches to seismic and flood risk management in UBEs, particularly within complex and historically stratified contexts. Due to its capabilities, this work can support the development of risk urban management strategies to be more effective and context-sensitive. This perspective can enhance adaptive planning and design of mitigation and risk-reduction interventions, starting from their disaster-specific allocation and their combination, too, and incorporating risk factors in the multi-layer single-risk perspectives to overcome the fragmentation of current approaches [27,29,80]. The focus on public open spaces and, in particular, on UBE hot-spots, could better optimise efforts and intervention costs, defining informed prioritisation rules by decision makers and local authorities.

From the perspective of risk management, planning and mitigation, future developments could explicitly integrate flood early warning-based storylines [11,21,36,117]. In line with reference approaches in flood risk and evacuation modelling (discussed before), early warning activation can be modelled by modifying not only the exposure parameter *E*, but also the vulnerability of users by their position (UVp_f). In this sense, when warnings are issued sufficiently in advance, users may evacuate earlier or move to upper floors, thus mainly reducing the number of individuals located in undergrounds, ground floors or outdoor spaces. As demonstrated in storyline-based flood modelling approaches [11,36,117], such assumptions can be incorporated by creating alternative temporal scenarios with reduced occupant loads in exposed areas, or with different distributions of user types depending on the warning level and behavioural response. Such storyline-based adjustments would account for the mitigating role of forecasts and alerts, while remaining coherent with its scenario-based and spatiotemporal structure [117].

Furthermore, the current deterministic approach could be integrated into future applications by probabilistic fragility functions. This would allow accounting for variability in damage among buildings with the same hazard intensity and vulnerability, differentiating macro-building classes, construction age, masonry sub-typologies, or effectiveness of retrofitting solutions (including anti-seismic devices). Such refinements would complement the operational matrix with probabilistic damage estimates, increasing accuracy while maintaining the scenario-based and meso-scale consistency of the framework moving from risk assessment to mitigation [46]. This extension is particularly relevant for earthquake risk, by mainly considering pre-code historical buildings, where deterministic assignment of Limit States [36] may be less precise, enabling a more nuanced representation of potential damage for urban-scale risk management. Similarly, considering earthquake risks, future works could also improve the damage assessment reliability by: (a) extending and adapting the *Ivs* assessment methodology to other construction types (such as reinforced concrete or mixed typologies), by appropriately calibrating parameters and vulnerability classes according to materials, structural systems, and code levels; (b) include the relevance of local amplification phenomena by including microzonation inputs and finer-scale PGA maps in the assessment process. Concerning point (b), indeed, the framework can readily integrate local amplification factors as a function of soil classes or distance from the river, in line with existing literature on river-related site effects.

Finally, the applications of the methodology should be extended to other relevant contexts, including both historical and modern UBEs, in different Countries, with occupancy loads adapted to local conditions. This would strengthen the validation of the approach and promote further modifications and integrations. In this sense, the framework is inherently scalable and transferable, and its application beyond the initial case study (particularly in cities with similar morphological or functional characteristics) could support the diffusion of standardised procedures and shared analytical tools. This would promote the establishment of a common foundation for multiscale urban risk assessment, helping cities build resilience through evidence-based planning and adaptive risk management.

CRediT authorship contribution statement

Enrico Quagliarini: Writing – review & editing, Validation, Supervision, Resources, Project administration, Methodology, Funding acquisition, Conceptualization. **Alessia Freddo:** Writing – original draft, Validation, Software, Investigation. **Caterina Alighieri:** Writing – original draft, Visualization, Methodology, Investigation, Formal analysis, Data curation. **Maud Natalucci:** Writing – original draft, Visualization, Methodology, Investigation, Formal analysis, Data curation. **Gabriele Bernardini:** Writing – original draft, Validation, Supervision, Methodology, Conceptualization.

Declaration of competing interest

The authors declare that they have no known competing financial interests or personal relationships that could have appeared to influence the work reported in this paper.

Acknowledgement

This research has received funding under the project ReACT ("(planning) Resilient urban and metropolitAn built environments through inClusive mulTi-risk behavioural-based models and simulations", project code PE0000005, CUP E63C22002000002 – funded under the National Recovery and Resilience Plan (NRRP), Mission 4 Component 2 Investment 1.3 ('Partenariati estesi alle università, ai centri di ricerca, alle aziende per il finanziamento di progetti di ricerca di base') funded by the European Union – NextGenerationEU, Italian Ministry of University, according to the Call for tender "Decreto Direttoriale No. 341 of March 15, 2022", Project "Multi-Risk sciEnce for resilienT commUnities undeR a changiNg climate (RETURN)", code PE0000005 – CUP, Concession Decree (Decreto Direttoriale) No. 1552 of October 11, 2022, within the "BANDO a CASCATA" of Spoke 5 TS1 "Insediamenti Urbani e Metropolitani", with relation to the ReACT Concession Decree (Decreto Rettorale di concessione del finanziamento) DR/2025/107 of January 13, 2025 from Università Federico II di Napoli as Spoke.

Appendix A. Supplementary data

Supplementary data to this article can be found online at https://doi.org/10.1016/j.ijdrr.2026.106072.

Appendix A

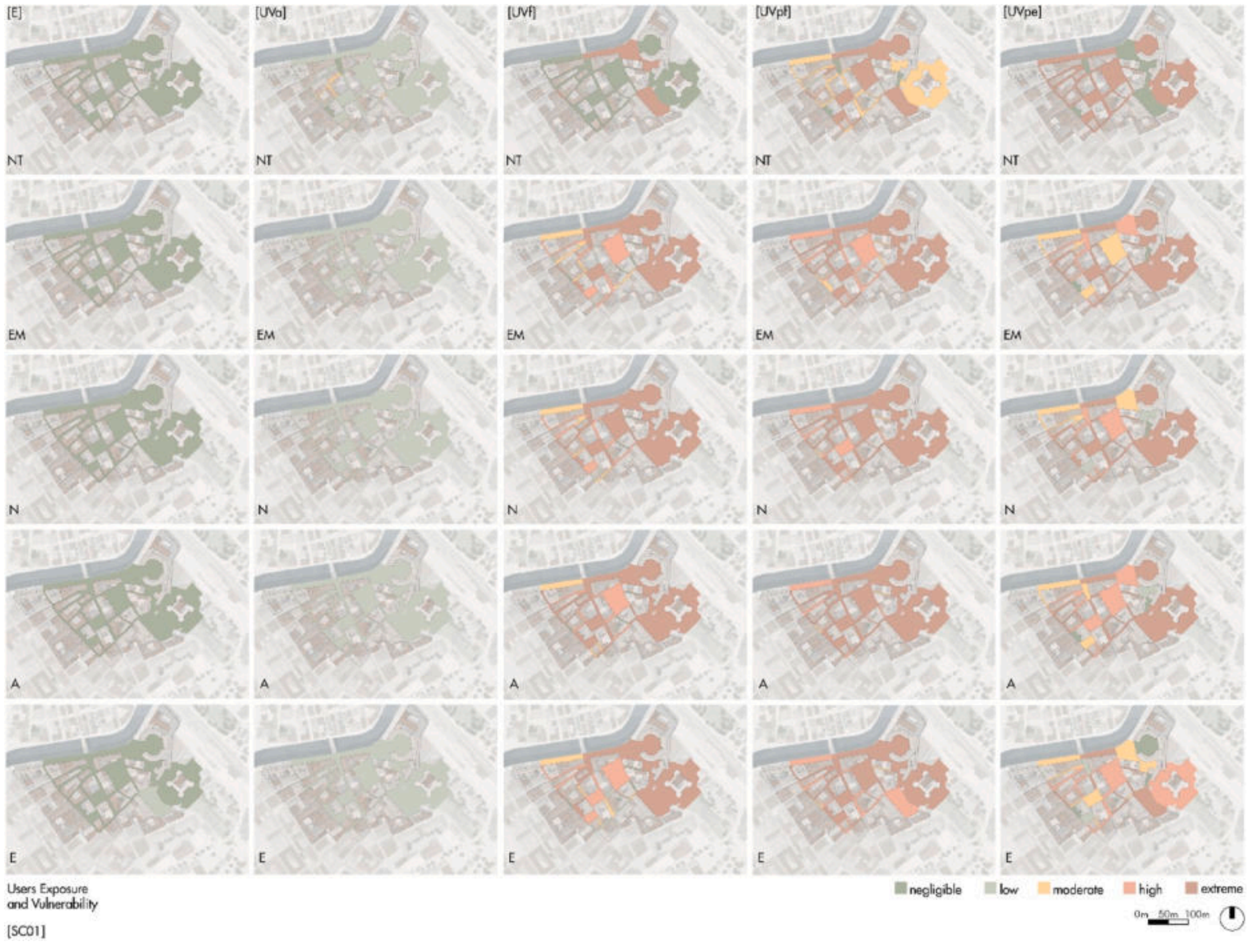

Fig. A.1. Maps over time of *E, UVa, UVf,* UVp_f and UVp_e, for SC01.

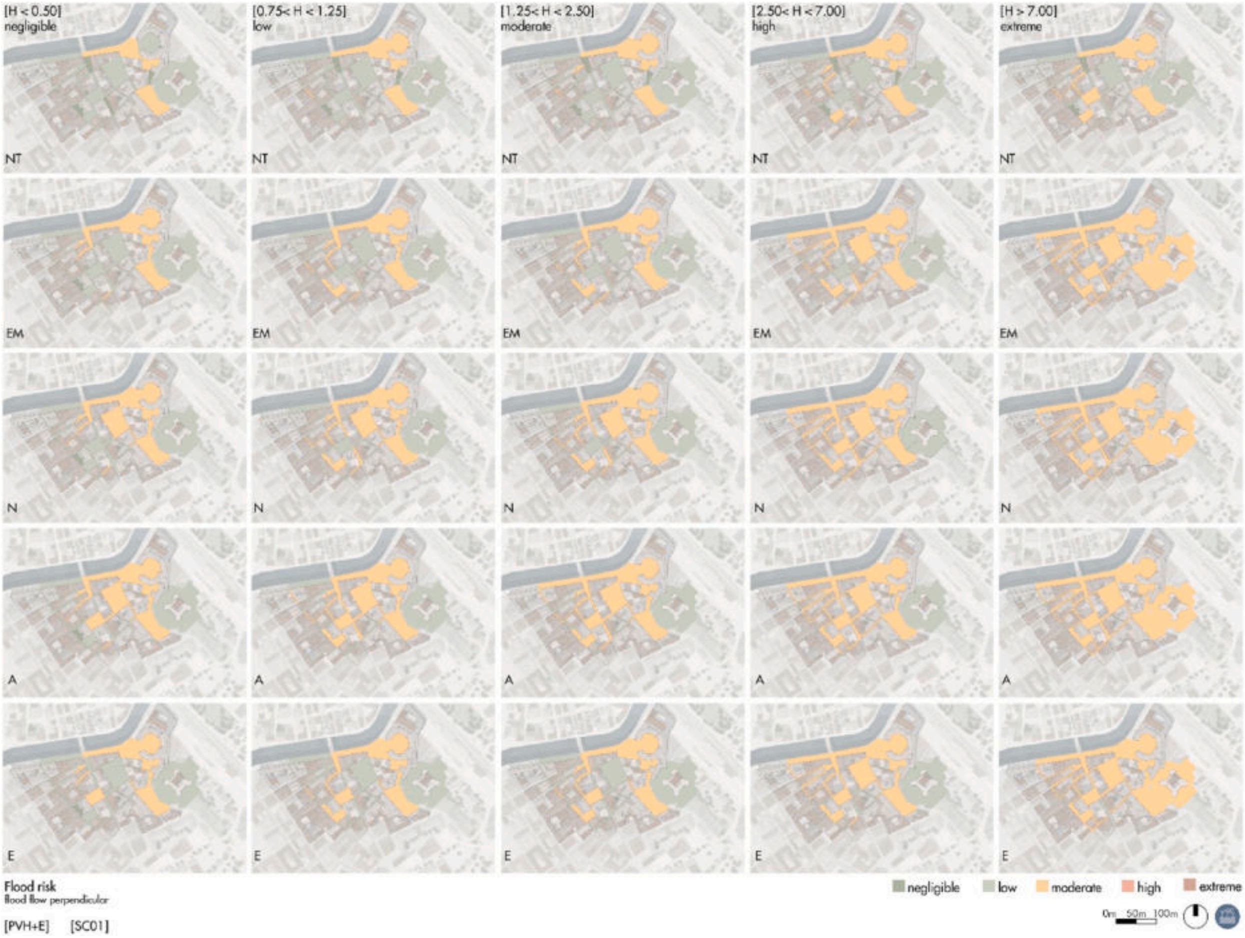

Fig. A.2. Maps over time of single risk for flood at the open space scale in SC01, depending on *H* scenarios, and considering floodwater flow perpendicular to the river axis.

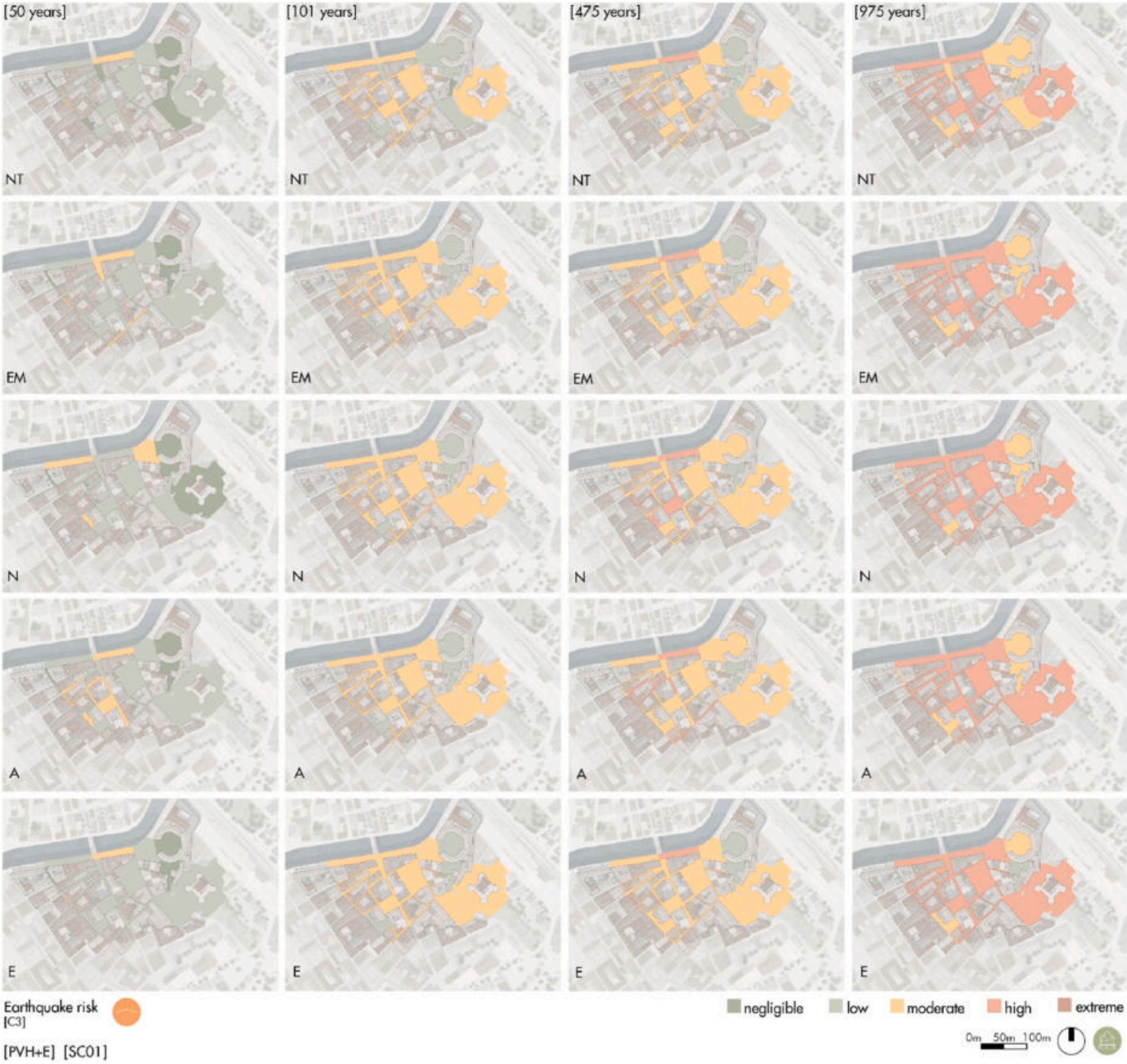

Fig. A.3. Maps over time of single risk for earthquake at the open space scale in SC01, depending on *H* scenarios (50, 101, 475 and 975 years), and considering C3 for *PV* conditions.

9 Appendix B

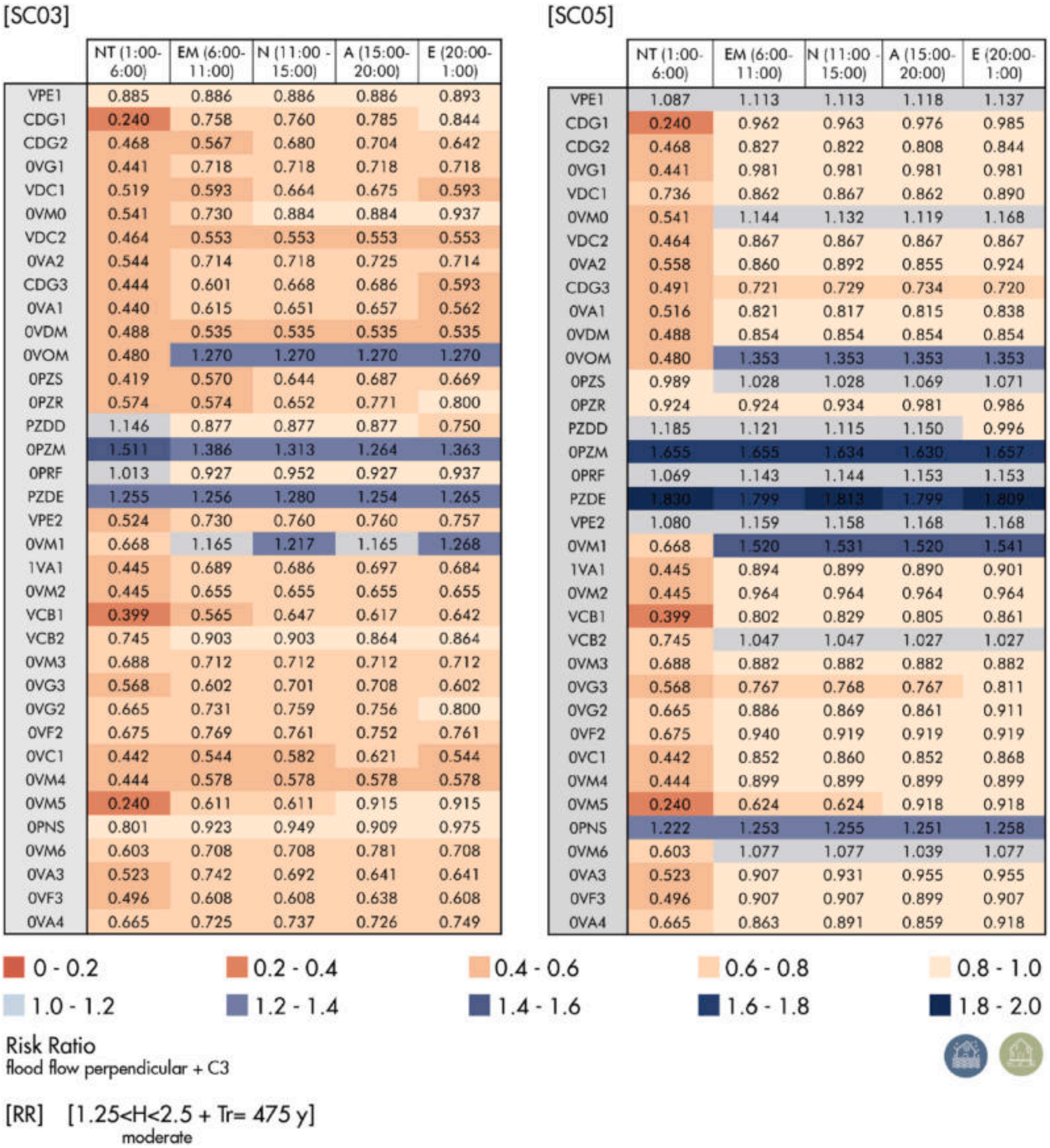
[SC03]

	NT (1:00-6:00)	EM (6:00-11:00)	N (11:00 - 15:00)	A (15:00-20:00)	E (20:00-1:00)
VPE1	0.885	0.886	0.886	0.886	0.893
CDG1	0.240	0.758	0.760	0.785	0.844
CDG2	0.468	0.567	0.680	0.704	0.642
0VG1	0.441	0.718	0.718	0.718	0.718
VDC1	0.519	0.593	0.664	0.675	0.593
0VM0	0.541	0.730	0.884	0.884	0.937
VDC2	0.464	0.553	0.553	0.553	0.553
0VA2	0.544	0.714	0.718	0.725	0.714
CDG3	0.444	0.601	0.668	0.686	0.593
0VA1	0.440	0.615	0.651	0.657	0.562
0VDM	0.488	0.535	0.535	0.535	0.535
0VOM	0.480	1.270	1.270	1.270	1.270
0PZS	0.419	0.570	0.644	0.687	0.669
0PZR	0.574	0.574	0.652	0.771	0.800
PZDD	1.146	0.877	0.877	0.877	0.750
0PZM	1.511	1.386	1.313	1.264	1.363
0PRF	1.013	0.927	0.952	0.927	0.937
PZDE	1.255	1.256	1.280	1.254	1.265
VPE2	0.524	0.730	0.760	0.760	0.757
0VM1	0.668	1.165	1.217	1.165	1.268
1VA1	0.445	0.689	0.686	0.697	0.684
0VM2	0.445	0.655	0.655	0.655	0.655
VCB1	0.399	0.565	0.647	0.617	0.642
VCB2	0.745	0.903	0.903	0.864	0.864
0VM3	0.688	0.712	0.712	0.712	0.712
0VG3	0.568	0.602	0.701	0.708	0.602
0VG2	0.665	0.731	0.759	0.756	0.800
0VF2	0.675	0.769	0.761	0.752	0.761
0VC1	0.442	0.544	0.582	0.621	0.544
0VM4	0.444	0.578	0.578	0.578	0.578
0VM5	0.240	0.611	0.611	0.915	0.915
0PNS	0.801	0.923	0.949	0.909	0.975
0VM6	0.603	0.708	0.708	0.781	0.708
0VA3	0.523	0.742	0.692	0.641	0.641
0VF3	0.496	0.608	0.608	0.638	0.608
0VA4	0.665	0.725	0.737	0.726	0.749

[SC05]

	NT (1:00-6:00)	EM (6:00-11:00)	N (11:00 - 15:00)	A (15:00-20:00)	E (20:00-1:00)
VPE1	1.087	1.113	1.113	1.118	1.137
CDG1	0.240	0.962	0.963	0.976	0.985
CDG2	0.468	0.827	0.822	0.808	0.844
0VG1	0.441	0.981	0.981	0.981	0.981
VDC1	0.736	0.862	0.867	0.862	0.890
0VM0	0.541	1.144	1.132	1.119	1.168
VDC2	0.464	0.867	0.867	0.867	0.867
0VA2	0.558	0.860	0.892	0.855	0.924
CDG3	0.491	0.721	0.729	0.734	0.720
0VA1	0.516	0.821	0.817	0.815	0.838
0VDM	0.488	0.854	0.854	0.854	0.854
0VOM	0.480	1.353	1.353	1.353	1.353
0PZS	0.989	1.028	1.028	1.069	1.071
0PZR	0.924	0.924	0.934	0.981	0.986
PZDD	1.185	1.121	1.115	1.150	0.996
0PZM	1.655	1.655	1.634	1.630	1.657
0PRF	1.069	1.143	1.144	1.153	1.153
PZDE	1.830	1.799	1.813	1.799	1.809
VPE2	1.080	1.159	1.158	1.168	1.168
0VM1	0.668	1.520	1.531	1.520	1.541
1VA1	0.445	0.894	0.899	0.890	0.901
0VM2	0.445	0.964	0.964	0.964	0.964
VCB1	0.399	0.802	0.829	0.805	0.861
VCB2	0.745	1.047	1.047	1.027	1.027
0VM3	0.688	0.882	0.882	0.882	0.882
0VG3	0.568	0.767	0.768	0.767	0.811
0VG2	0.665	0.886	0.869	0.861	0.911
0VF2	0.675	0.940	0.919	0.919	0.919
0VC1	0.442	0.852	0.860	0.852	0.868
0VM4	0.444	0.899	0.899	0.899	0.899
0VM5	0.240	0.624	0.624	0.918	0.918
0PNS	1.222	1.253	1.255	1.251	1.258
0VM6	0.603	1.077	1.077	1.039	1.077
0VA3	0.523	0.907	0.931	0.955	0.955
0VF3	0.496	0.907	0.907	0.899	0.907
0VA4	0.665	0.863	0.891	0.859	0.918

Fig. B.1. Comparison of the *RR* values for the SC03 and SC05 in association with Fig. 18.

Data availability

Main data to support results are reported in the document, appendices and supplementary materials. Additional data will be available on reasonable request.

References

[1] X. Shu, C. Ye, Z. Xu, R. Liao, S. Zhang, A multiscale physically-based approach to urban flood risk assessment using ABM and multi-source remote sensing data, Int. J. Disaster Risk Reduct. 119 (2025) 105332, https://doi.org/10.1016/j.ijdrr.2025.105332.

[2] E.Y. Menteşe, G. Cremen, R. Gentile, C. Galasso, M.E. Filippi, J. McCloskey, Future exposure modelling for risk-informed decision making in urban planning, Int. J. Disaster Risk Reduct. 90 (2023) 103651, https://doi.org/10.1016/j.ijdrr.2023.103651.

[3] Q. Guo, S. Jiao, Y. Yang, Y. Yu, Y. Pan, Assessment of urban flood disaster responses and causal analysis at different temporal scales based on social media data and machine learning algorithms, Int. J. Disaster Risk Reduct. 117 (2025) 105170, https://doi.org/10.1016/j.ijdrr.2024.105170.

[4] A. Sharifi, Resilience of urban social-ecological-technological systems (SETS): a review, Sustain. Cities Soc. 99 (2023) 104910, https://doi.org/10.1016/j.scs.2023.104910.
[5] A.C.R. Lopes, O.M. Rezende, M.G. Miguez, Urban resilience to floods in the context of the disaster risk management cycle: a literature review, J. Hydrol. 662 (2025) 133827, https://doi.org/10.1016/j.jhydrol.2025.133827.
[6] A. Sakurai, T. Sato, Promoting education for disaster resilience and the sendai framework for disaster risk reduction, J. Disaster Res. 11 (2016) 402–412, https://doi.org/10.20965/jdr.2016.p0402.
[7] UNDRR, Sendai framework for disaster risk reduction 2015-2030. http://files/12384/UNDRR-2015-SendaiFrameworkforDisasterRiskReduction2015-2030.pdf, 2015.
[8] UNDRR, A/RES/71/644 Report of the open-ended intergovernmental expert working group on indicators and terminology relating to disaster risk reduction (2016). https://www.preventionweb.net/publication/report-open-ended-intergovernmental-expert-working-group-indicators-and-terminology.
[9] E.L. French, S.J. Birchall, K. Landman, R.D. Brown, Designing public open space to support seismic resilience: a systematic review, Int. J. Disaster Risk Reduct. 34 (2019) 1–10, https://doi.org/10.1016/j.ijdrr.2018.11.001.
[10] A. Unwfp, Guide for Vulnerability and Spatial Analysis in sudden-onset Disasters, 2018.
[11] Federal emergency management agency (FEMA), hazus flood model, Technical Manual - Hazus 6.1, https://www.fema.gov/sites/default/files/documents/fema_hazus-flood-model-technical-manual-6-1.pdf, 2024.
[12] T. Tingsanchali, Urban flood disaster management, Procedia Eng. 32 (2012) 25–37, https://doi.org/10.1016/j.proeng.2012.01.1233.
[13] G. Zuccaro, M.F. Leone, C. Martucci, Future research and innovation priorities in the field of natural hazards, disaster risk reduction, disaster risk management and climate change adaptation: a shared vision from the ESPREsSO project, Int. J. Disaster Risk Reduct. 51 (2020) 101783, https://doi.org/10.1016/j.ijdrr.2020.101783.
[14] Y. Zang, J. Huang, H. Wang, Dynamic impact assessment of urban floods on the compound spatial network of buildings-roads-emergency service facilities, Sci. Total Environ. 926 (2024) 172007, https://doi.org/10.1016/j.scitotenv.2024.172007.
[15] F. Giuliani, A. De Falco, V. Cutini, Unpacking seismic risk in Italian historic centres: a critical overview for disaster risk reduction, Int. J. Disaster Risk Reduct. 59 (2021) 102260, https://doi.org/10.1016/j.ijdrr.2021.102260.
[16] Z. Ahmadi, M. Ghasemi, A.R. Khavarian-Garmsir, M. Ahmadi, Integrating flood and earthquake resilience: a framework for assessing urban community resilience against multiple hazards, J. Saf. Sci. Resil. 5 (2024) 330–343, https://doi.org/10.1016/j.jnlssr.2024.05.002.
[17] S. Fischer, A.H. Schumann, Dominant flood types in Europe and their role in flood statistics, Hydrol. Sci. J. (2025) 1–17, https://doi.org/10.1080/02626667.2025.2450369.
[18] C. Bianchi, P. Salvati, Rapporto Periodico sul Rischio posto alla Popolazione italiana da Frane e inondazioni - anno 2023. https://doi.org/10.30437/report2023, 2024.
[19] M. Wyss, M. Speiser, S. Tolis, Earthquake fatalities and potency, Nat. Hazards 119 (2023) 1091–1106, https://doi.org/10.1007/s11069-022-05627-x.
[20] UCLouvain, CRED, USAID, 2023 Disaster in Numbers, 2023. https://files.emdat.be/reports/2023_EMDAT_report.pdf.
[21] Q. Dai, X. Zhu, L. Zhuo, D. Han, Z. Liu, S. Zhang, A hazard-human coupled model (HazardCM) to assess city dynamic exposure to rainfall-triggered natural hazards, Environ. Model. Software 127 (2020) 104684, https://doi.org/10.1016/j.envsoft.2020.104684.
[22] P. He, D. Zhang, W. Chen, B. Jia, Spatio-temporal distribution estimation and analysis of post-earthquake casualties in urban areas: a case study in chenghua district, chengdu, Int. J. Disaster Risk Reduct. 123 (2025) 105477, https://doi.org/10.1016/j.ijdrr.2025.105477.
[23] H. Chen, Z. Xu, Y. Liu, Y. Huang, F. Yang, Urban flood risk assessment based on dynamic population distribution and fuzzy comprehensive evaluation, Int. J. Environ. Res. Publ. Health 19 (2022) 16406, https://doi.org/10.3390/ijerph192416406.
[24] X. Duan, W. Fei, Assessment of the impact of temporal and spatial factors on the emergency evacuation capacity of external spaces in high-density urban communities during earthquake disasters, Int. J. Disaster Risk Reduct. (2025) 105760, https://doi.org/10.1016/j.ijdrr.2025.105760.
[25] E. Quagliarini, G. Bernardini, G. Romano, M. D'Orazio, Users' vulnerability and exposure in Public Open Spaces (squares): a novel way for accounting them in multi-risk scenarios, Cities 133 (2023) 104160, https://doi.org/10.1016/j.cities.2022.104160.
[26] Y. Shi, Q. Yao, J. Wen, J. Xi, H. Li, Q. Wang, A spatial accessibility assessment of urban tourist attractions emergency response in Shanghai, Int. J. Disaster Risk Reduct. 74 (2022) 102919, https://doi.org/10.1016/j.ijdrr.2022.102919.
[27] K. Renner, S. Schneiderbauer, F. Pruß, C. Kofler, D. Martin, S. Cockings, Spatio-temporal population modelling as improved exposure information for risk assessments tested in the Autonomous Province of Bolzano, Int. J. Disaster Risk Reduct. 27 (2018) 470–479, https://doi.org/10.1016/j.ijdrr.2017.11.011.
[28] J. Dabbeek, H. Crowley, V. Silva, S. Ozcebe, Impact of population spatiotemporal patterns on earthquake human losses, Int. J. Disaster Risk Reduct. 122 (2025) 105455, https://doi.org/10.1016/j.ijdrr.2025.105455.
[29] M. Polese, G. Tocchi, A. Babič, M. Dolšek, M. Faravelli, D. Quaroni, B. Borzi, N. Rebora, D. Ottonelli, S. Wernhart, J. Pejovic, N. Serdar, K. Lebar, S. Rusjan, R. Masi, C. Resch, H. Kern, I. Cipranić, M. Ostojic, A. Prota, Multi-risk assessment in transboundary areas: a framework for harmonized evaluation considering seismic and flood risks, Int. J. Disaster Risk Reduct. 101 (2024) 104275, https://doi.org/10.1016/j.ijdrr.2024.104275.
[30] L. Zhao, F. He, C. Zhao, A framework of resilience development for poor villages after the wenchuan earthquake based on the principle of "build back better,", Sustainability 12 (2020) https://doi.org/10.3390/su12124979.
[31] C. Galasso, J. McCloskey, M. Pelling, M. Hope, C.J. Bean, G. Cremen, R. Guragain, U. Hancilar, J. Menoscal, K. Mwang'a, J. Phillips, D. Rush, H. Sinclair, Editorial. Risk-based, pro-poor urban design and planning for tomorrow's cities, Int. J. Disaster Risk Reduct. 58 (2021) 102158, https://doi.org/10.1016/j.ijdrr.2021.102158.
[32] G. Fernandez, I. Ahmed, "Build back better" approach to disaster recovery: research trends since 2006, Prog. Disaster Sci. 1 (2019) 100003, https://doi.org/10.1016/j.pdisas.2019.100003.
[33] E. Quagliarini, G. Bernardini, L. Domenella, G. Marinelli, Supporting "Build Back Better" in historical towns: a novel methodology to include users' exposure and vulnerability in strategic function relocation assessment, Int. J. Disaster Risk Reduct. 127 (2025) 105700, https://doi.org/10.1016/j.ijdrr.2025.105700.
[34] C. Galasso, E.A. Opabola, The 2023 Kahramanmaraş Earthquake Sequence: finding a path to a more resilient, sustainable, and equitable society, Commun. Eng. 3 (2024) 24, https://doi.org/10.1038/s44172-024-00170-y.
[35] M.-H. Graveline, D. Germain, Disaster risk resilience: conceptual evolution, key issues, and opportunities, Int. J. Disaster Risk Sci. 13 (2022) 330–341, https://doi.org/10.1007/s13753-022-00419-0.
[36] S. Opper, P. Cinque, B. Davies, Timeline modelling of flood evacuation operations, Procedia Eng. 3 (2010) 175–187, https://doi.org/10.1016/j.proeng.2010.07.017.
[37] J. Zschau, Where are we with multihazards , multirisks assessment capacities, in: Science for Disaster Risk Management 2017: Knowing Better and Losing less, European Commission, 2017, pp. 98–130. https://drmkc.jrc.ec.europa.eu/portals/0/Knowledge/ScienceforDRM/ch02/ch02_subch0205.pdf.
[38] J. Hielkema, Laura; Suidman, Multi-Hazard Risk Analysis Methodologies, Anticipation Hub, 2021, pp. 1–9.
[39] A. Sharifi, Resilient urban forms: a review of literature on streets and street networks, Build. Environ. 147 (2019) 171–187, https://doi.org/10.1016/j.buildenv.2018.09.040.
[40] A. Sharifi, Resilient urban forms: a macro-scale analysis, Cities 85 (2019) 1–14, https://doi.org/10.1016/j.cities.2018.11.023.
[41] G. Bernardini, T.M. Ferreira, P. Baquedano Julià, R. Ramírez Eudave, E. Quagliarini, Assessing the spatiotemporal impact of users' exposure and vulnerability to flood risk in urban built environments, Sustain. Cities Soc. 100 (2024) 105043, https://doi.org/10.1016/j.scs.2023.105043.
[42] Y. Cao, C. Xu, N.M. Aziz, S.N. Kamaruzzaman, BIM–GIS integrated utilization in urban disaster management: the contributions, challenges, and future directions, Remote Sens. 15 (2023) 1331, https://doi.org/10.3390/rs15051331.
[43] A. Sharifi, Urban form resilience: a meso-scale analysis, Cities 93 (2019) 238–252, https://doi.org/10.1016/j.cities.2019.05.010.
[44] F.N. Miranda, T.M. Ferreira, A simplified approach for flood vulnerability assessment of historic sites, Nat. Hazards 96 (2019) 713–730, https://doi.org/10.1007/s11069-018-03565-1.

[45] L. Davis, T. Larionova, D. Patel, D. Tse, P. Baquedano Juliá, P. Pinto Santos, T.M. Ferreira, Flood vulnerability and risk assessment of historic urban areas: vulnerability evaluation, derivation of depth-damage curves and cost–benefit analysis of flood adaptation measures applied to the historic city centre of Tomar, Portugal, J. Flood Risk Manag. 16 (2023) 1–18, https://doi.org/10.1111/jfr3.12908.
[46] L. Bernabei, G. Mochi, G. Bernardini, E. Quagliarini, Seismic risk of Open Spaces in Historic built Environments: a matrix-based approach for emergency management and disaster response, Int. J. Disaster Risk Reduct. 65 (2021) 102552, https://doi.org/10.1016/j.ijdrr.2021.102552.
[47] K. McClymont, M. Bedinger, L. Beevers, A. Visser-Quinn, G.H. Walker, Understanding urban resilience with the urban systems abstraction hierarchy (USAH), Sustain. Cities Soc. 80 (2022) 103729, https://doi.org/10.1016/j.scs.2022.103729.
[48] M.Z. Memluk, Designing urban squares, in: Advances in Landscape Architecture, InTech, 2013, https://doi.org/10.5772/55826.
[49] B. Evans, A. Lam, C. West, R. Ahmadian, S. Djordjević, A. Chen, M. Pregnolato, A combined stability function to quantify flood risks to pedestrians and vehicle occupants, Sci. Total Environ. 908 (2024) 168237, https://doi.org/10.1016/j.scitotenv.2023.168237.
[50] M.B. Rojo, E. Beck, C. Lutoff, The street as an area of human exposure in an earthquake aftermath: the case of Lorca, Spain, 2011, Nat. Hazards Earth Syst. Sci. 17 (2017) 581–594, https://doi.org/10.5194/nhess-17-581-2017.
[51] J.C. Villagràn De León, Vulnerability: a Conceptual and Methodological Review, 2006. http://collections.unu.edu/eserv/UNU:1871/pdf3904.pdf.
[52] H. Badreldin, C. Scaini, H.M. Hassan, A. Peresan, High-resolution multi-hazard residential buildings and population exposure model for coastal areas: a case study in northeastern Italy, Int. J. Disaster Risk Reduct. 121 (2025) 105403, https://doi.org/10.1016/j.ijdrr.2025.105403.
[53] H. Aghamohammadi, M.S. Mesgari, A. Mansourian, D. Molaei, Seismic human loss estimation for an earthquake disaster using neural network, Int. J. Environ. Sci. Technol. 10 (2013) 931–939, https://doi.org/10.1007/s13762-013-0281-5.
[54] R. Ponce-Lopez, J. Ferreira, Identifying and characterizing popular non-work destinations by clustering cellphone and point-of-interest data, Cities 113 (2021) 103158, https://doi.org/10.1016/j.cities.2021.103158.
[55] J. Dibble, A. Prelorendjos, O. Romice, M. Zanella, E. Strano, M. Pagel, S. Porta, On the origin of spaces: morphometric foundations of urban form evolution, Environ. Plan. B Urban Anal. City Sci. 46 (2019) 707–730, https://doi.org/10.1177/2399808317725075.
[56] R. Roussel, S. Jacoby, A. Asadipour, Robust building identification from street views using deep convolutional neural networks, Buildings 14 (2024) 1–26, https://doi.org/10.3390/buildings14030578.
[57] Y. Kim, T. Carvalhaes, A. Helmrich, S. Markolf, R. Hoff, M. Chester, R. Li, N. Ahmad, Leveraging SETS resilience capabilities for safe-to-fail infrastructure under climate change, Curr. Opin. Environ. Sustain. 54 (2022) 101153, https://doi.org/10.1016/j.cosust.2022.101153.
[58] V. Shirvani Harandi, K. Amini Hosseini, B. Mansouri, Assessing the effect of physical and social parameters on seismic risk of urban transportation networks, Int. J. Disaster Risk Reduct. 101 (2024) 104269, https://doi.org/10.1016/j.ijdrr.2024.104269.
[59] T.M. Ferreira, P.P. Santos, An integrated approach for assessing flood risk in historic City centres, Water 12 (2020) 1648, https://doi.org/10.3390/w12061648.
[60] F. Giuliani, A. De Falco, V. Cutini, The role of urban configuration during disasters. A scenario-based methodology for the post-earthquake emergency management of Italian historic centres, Saf. Sci. 127 (2020) 104700, https://doi.org/10.1016/j.ssci.2020.104700.
[61] F. Giuliani, A. De Falco, V. Cutini, Rethinking earthquake-related vulnerabilities of historic centres in Italy: insights from the Tuscan area, J. Cult. Herit. 54 (2022) 79–93, https://doi.org/10.1016/j.culher.2022.01.004.
[62] R. Maio, T.M. Ferreira, R. Vicente, A critical discussion on the earthquake risk mitigation of urban cultural heritage assets, Int. J. Disaster Risk Reduct. 27 (2018) 239–247, https://doi.org/10.1016/j.ijdrr.2017.10.010.
[63] E.E. Koks, B. Jongman, T.G. Husby, W.J.W. Botzen, Combining hazard, exposure and social vulnerability to provide lessons for flood risk management, Environ. Sci. Pol. 47 (2015) 42–52, https://doi.org/10.1016/j.envsci.2014.10.013.
[64] P. Lonetti, R. Maletta, Dynamic impact analysis of masonry buildings subjected to flood actions, Eng. Struct. 167 (2018) 445–458, https://doi.org/10.1016/j.engstruct.2018.03.076.
[65] T. Mohd, M.H. Mohamed Saraf, S.F. Che Pin, M.N. Hasbullah, T.E. Nordin, D. Ismail, The degree of housing damage model for a flood affected area, MATEC Web Confer. 66 (2016) 00074, https://doi.org/10.1051/matecconf/20166600074.
[66] S. Soares-Frazão, J. Lhomme, V. Guinot, Y. Zech, Two-dimensional shallow-water model with porosity for urban flood modelling, J. Hydraul. Res. 46 (2008) 45–64, https://doi.org/10.1080/00221686.2008.9521842.
[67] European Commission, European overview assessment of member states ' reports on preliminary flood risk assessment and identification of areas of potentially significant flood risk. https://doi.org/10.2779/576456, 2015.
[68] A.K. Jha, R. Bloch, J. Lamond, Cities and Flooding, The World Bank, 2012, https://doi.org/10.1596/978-0-8213-8866-2.
[69] H. Ren, B. Pang, G. Zhao, Y. Liu, H. Zhang, S. Liu, Rapid flood simulation and source area identification in urban environments via interpretable deep learning, J. Hydrol. 651 (2025) 132551, https://doi.org/10.1016/j.jhydrol.2024.132551.
[70] S. Mobini, B. Pirzamanbein, R. Berndtsson, R. Larsson, Urban flood damage claim analyses for improved flood damage assessment, Int. J. Disaster Risk Reduct. 77 (2022) 103099, https://doi.org/10.1016/j.ijdrr.2022.103099.
[71] L.B.L. da Silva, J.S. Humberto, M.H. Alencar, R.J.P. Ferreira, A.T. de Almeida, GIS-based multidimensional decision model for enhancing flood risk prioritization in urban areas, Int. J. Disaster Risk Reduct. 48 (2020) 101582, https://doi.org/10.1016/j.ijdrr.2020.101582.
[72] E. Mignot, L. Camusson, N. Riviere, Measuring the flow intrusion towards building areas during urban floods: impact of the obstacles located in the streets and on the facade, J. Hydrol. 583 (2020) 124607, https://doi.org/10.1016/j.jhydrol.2020.124607.
[73] E. Mignot, X. Li, B. Dewals, Experimental modelling of urban flooding: a review, J. Hydrol. 568 (2019) 334–342, https://doi.org/10.1016/j.jhydrol.2018.11.001.
[74] H. Chang, A. Pallathadka, J. Sauer, N.B. Grimm, R. Zimmerman, C. Cheng, D.M. Iwaniec, Y. Kim, R. Lloyd, T. McPhearson, B. Rosenzweig, T. Troxler, C. Welty, R. Brenner, P. Herreros-Cantis, Assessment of urban flood vulnerability using the social-ecological-technological systems framework in six US cities, Sustain. Cities Soc. 68 (2021), https://doi.org/10.1016/j.scs.2021.102786.
[75] R. Agliata, A. Bortone, L. Mollo, The impact of the aggregation formula on indicator-based method for the assessment of building susceptibility to hydro-meteorological hazards, Int. J. Disaster Risk Reduct. 72 (2022) 102850, https://doi.org/10.1016/j.ijdrr.2022.102850.
[76] A. Altindal, S. Karimzadeh, M.A. Erberik, A. Askan, O. Anil, M.K. Kockar, M. Sahmaran, A case study for probabilistic seismic risk assessment of earthquake-prone old urban centers, Int. J. Disaster Risk Reduct. 61 (2021) 102376, https://doi.org/10.1016/j.ijdrr.2021.102376.
[77] Y. He, C. Zhai, W. Wen, C. Zhang, Probabilistic prediction of post-earthquake rubble distribution range for masonry structures, J. Build. Eng. 95 (2024) 110208, https://doi.org/10.1016/j.jobe.2024.110208.
[78] Y. Hosseini, R.K. Mohammadi, T.Y. Yang, A comprehensive approach in post-earthquake blockage prediction of urban road network and emergency resilience optimization, Reliab. Eng. Syst. Saf. 244 (2024) 109887, https://doi.org/10.1016/j.ress.2023.109887.
[79] R. Hassanzadeh, Earthquake population loss estimation using spatial modelling and survey data: the Bam earthquake, 2003, Iran, Soil Dynam. Earthq. Eng. 116 (2019) 421–435, https://doi.org/10.1016/j.soildyn.2018.09.023.
[80] E. Pilone, P. Mussini, M. Demichela, G. Camuncoli, Municipal emergency plans in Italy: requirements and drawbacks, Saf. Sci. 85 (2016) 163–170, https://doi.org/10.1016/j.ssci.2015.12.029.
[81] Z. Jiang, Q. Su, Y. Cui, Discussion on the coupling relationship between flood risk and population vulnerability from climate justice, J. Water Clim. Change 15 (2024) 1076–1090, https://doi.org/10.2166/wcc.2024.480.
[82] A. Galderisi, G. Limongi, A comprehensive assessment of exposure and vulnerabilities in multi-hazard urban environments: a key tool for risk-informed planning strategies, Sustainability 13 (2021) 9055, https://doi.org/10.3390/su13169055.
[83] Y. Song, L. Guo, C. Wang, J. Zhu, Z. Li, Urban road waterlogging multi-level assessment integrated flood models and road network models, Transport. Res. Transport Environ. 133 (2024) 104305, https://doi.org/10.1016/j.trd.2024.104305.
[84] R. Aghataher, H. Rabieifar, N.N. Samany, H. Rezayan, The suitability mapping of an urban spatial structure for earthquake disaster response using a gradient rain optimization algorithm (GROA), Heliyon 9 (2023) e20525, https://doi.org/10.1016/j.heliyon.2023.e20525.

[85] Y. Wang, A.S. Chen, G. Fu, S. Djordjević, C. Zhang, D.A. Savić, An integrated framework for high-resolution urban flood modelling considering multiple information sources and urban features, Environ. Model. Software 107 (2018) 85–95, https://doi.org/10.1016/j.envsoft.2018.06.010.
[86] M. Francini, S. Artese, S. Gaudio, A. Palermo, M.F. Viapiana, To support urban emergency planning: a GIS instrument for the choice of optimal routes based on seismic hazards, Int. J. Disaster Risk Reduct. 31 (2018) 121–134, https://doi.org/10.1016/j.ijdrr.2018.04.020.
[87] K. Khatooni, F. Hooshyaripor, B. MalekMohammadi, R. Noori, A new approach for urban flood risk assessment using coupled SWMM–HEC-RAS-2D model, J. Environ. Manag. 374 (2025) 123849, https://doi.org/10.1016/j.jenvman.2024.123849.
[88] W. Li, J. Yu, D. Chen, Y. Lin, R. Dong, X. Zhang, C. He, H. Fu, Fine-grained building function recognition with street-view images and GIS map data via geometry-aware semi-supervised learning, Int. J. Appl. Earth Obs. Geoinf. 137 (2025) 104386, https://doi.org/10.1016/j.jag.2025.104386.
[89] V. Chauhan, L. Gupta, J. Dixit, Machine learning and GIS-based multi-hazard risk modeling for Uttarakhand: integrating seismic, landslide, and flood susceptibility with socioeconomic vulnerability, Environ. Sustain. Indic. 26 (2025) 100664, https://doi.org/10.1016/j.indic.2025.100664.
[90] G. Wei, G.-S. Han, X. Lang, Using RS and GIS for risk management of natural disasters consequences: the case of cultural heritage in Jinan city, China, Heliyon 10 (2024) e38217, https://doi.org/10.1016/j.heliyon.2024.e38217.
[91] J. Dabbeek, V. Silva, C. Galasso, A. Smith, Probabilistic earthquake and flood loss assessment in the Middle East, Int. J. Disaster Risk Reduct. 49 (2020) 101662, https://doi.org/10.1016/j.ijdrr.2020.101662.
[92] Y. Chen, Q. Li, Scale-dependent exposure bias: assessing disaster risk in less economically developed regions, Int. J. Disaster Risk Reduct. 121 (2025) 105406, https://doi.org/10.1016/j.ijdrr.2025.105406.
[93] C. Curt, Multirisk: what trends in recent works? – a bibliometric analysis, Sci. Total Environ. 763 (2021) 142951, https://doi.org/10.1016/j.scitotenv.2020.142951.
[94] S. De Angeli, B.D. Malamud, L. Rossi, F.E. Taylor, E. Trasforini, R. Rudari, A multi-hazard framework for spatial-temporal impact analysis, Int. J. Disaster Risk Reduct. 73 (2022) 102829, https://doi.org/10.1016/j.ijdrr.2022.102829.
[95] A. Garcia-aristizabal, G.Z. Amra, M. Almeida, V. Reva, X.V. Adai, T. Rosqvist, M.P. Vtt, Dynamic Scenario Concept Models, 2013, https://doi.org/10.13140/RG.2.1.3609.7363.
[96] D. Jato-Espino, C. Manchado, A. Roldán-Valcarce, A compact multi-hazard assessment model to identify urban areas prone to heat islands, floods and particulate matter, Int. J. Disaster Risk Reduct. 119 (2025) 105277, https://doi.org/10.1016/j.ijdrr.2025.105277.
[97] A. Alves, Z. Vojinovic, Z. Kapelan, A. Sanchez, B. Gersonius, Exploring trade-offs among the multiple benefits of green-blue-grey infrastructure for urban flood mitigation, Sci. Total Environ. 703 (2020) 134980, https://doi.org/10.1016/j.scitotenv.2019.134980.
[98] A. Sharifi, Trade-offs and conflicts between urban climate change mitigation and adaptation measures: a literature review, J. Clean. Prod. 276 (2020) 122813, https://doi.org/10.1016/j.jclepro.2020.122813.
[99] Ministry of Interior (Italy), DM 03/08/2015: technical fire prevention standards (testo coordinato dell'allegato I del DM 3 agosto 2015 - codice di prevenzione incendi - release beta 3). https://www.vigilfuoco.it/allegati/PI/COORD_DM_03_08_2015_Codice_Prevenzione_Incendi.pdf, 2020.
[100] Burden Bloomberg, New York City Pedestrian Level of Service Study Phase I, 2006.
[101] FEMA, Risk Management Series Primer for Design Professionals, 2004.
[102] C. Meletti, V. Montaldo, Interactive Maps of Seismic Hazard (WebGis), Progetto DPC-INGV S1, 2007.
[103] Italian Ministry of Infrastructure and Transport, Ministerial Decree D.M. 20.02.2018 Updating of Technical Standards for Construction, Roma, 2018. https://www.gazzettaufficiale.it/eli/gu/2018/02/20/42/so/8/sg/pdf.
[104] G. Grünthal, European Macroseismic Scale 1998 (EMS-98), vol. 15, Cahiers du Centre Européen de Géodynamique et de Séismologie, 1998.
[105] L. Bernabei, G. Vaiano, F. Rosso, G. Mochi, A novel seismic vulnerability assessment of masonry façades: framing and validation on Caldarola case study after 2016 Central Italy earthquake, TEMA, Technol. En. Mater. Architect. (e-ISSN 2421-4574) (2021) 7, https://doi.org/10.30682/tema0702d.
[106] S. Giovinazzi, S. Lagomarsino, A macroseismic method for vulnerability assessment of buildings, in: Proceeding of The13th World Conference on Earthquake Engineering, Canada, Vancouver, B.C., 2004. http://www.iitk.ac.in/nicee/wcee/article/13_896.pdf.
[107] K.D. Goepel, METHOD FOR MULTI-CRITERIA DECISION MAKING IN CORPORATE 2 . AHP Spreadsheet Template 3 . Experiences in the practical application of AHP, Proceed. Int. Symp. Analytic Hierarchy Process 2 (2013) 1–10.
[108] K.D. Goepel, Implementation of an online software tool for the Analytic Hierarchy Process (AHP-OS), Int. J. Analy. Hierarchy Process 10 (2018), https://doi.org/10.13033/ijahp.v10i3.590.
[109] M. Papathoma-Köhle, Vulnerability curves vs. vulnerability indicators: application of an indicator-based methodology for debris-flow hazards, Nat. Hazards Earth Syst. Sci. 16 (2016) 1771–1790, https://doi.org/10.5194/nhess-16-1771-2016.
[110] L.L. Moreira, M.M. de Brito, M. Kobiyama, Review article: a systematic review and future prospects of flood vulnerability indices, Nat. Hazards Earth Syst. Sci. 21 (2021) 1513–1530, https://doi.org/10.5194/nhess-21-1513-2021.
[111] K.D. Goepel, Implementing the analytic hierarchy process as a standard method for multi-criteria decision making in corporate enterprises – a new AHP excel template with multiple inputs. https://doi.org/10.13033/isahp.y2013.047, 2013.
[112] A. FathiAzar, S. De Angeli, S. Cattari, Towards integrated multi-risk reduction strategies: a catalog of flood and earthquake risk mitigation measures at the building and neighborhood scales, Int. J. Disaster Risk Reduct. 113 (2024) 104884, https://doi.org/10.1016/j.ijdrr.2024.104884.
[113] D. Asadollahzadeh, B. Behnam, Machine learning approaches for seismic vulnerability assessment of urban buildings: a comparative study with analytic hierarchy process, Prog. Disaster Sci. 25 (2025) 100398, https://doi.org/10.1016/j.pdisas.2024.100398.
[114] D. Dai, M. Bo, X. Ren, K. Dai, Application and exploration of artificial intelligence technology in urban ecosystem-based disaster risk reduction: a scoping review, Ecol. Indic. 158 (2024) 111565, https://doi.org/10.1016/j.ecolind.2024.111565.
[115] R. Rodríguez, A. Robles-Morua, D. Meza-Figueroa, J. Tuxpan-Vargas, R. Cisneros Almazán, N. Perez Ramos, B. Sen-Gupta, N. Martínez-Villegas, Urban flood exposure assessment through citizen science, 2D hydraulic modeling, and artificial intelligence, J. Environ. Manag. 393 (2025) 127037, https://doi.org/10.1016/j.jenvman.2025.127037.
[116] W. Zhou, Y. Li, M. Gou, B. Wang, C. Fang, Urban spatial vulnerability analysis based on urban systems using support vector machine, Sustain. Cities Soc. 123 (2025) 106274, https://doi.org/10.1016/j.scs.2025.106274.
[117] K.M. de Bruijn, N. Lips, B. Gersonius, H. Middelkoop, The storyline approach: a new way to analyse and improve flood event management, Nat. Hazards 81 (2016) 99–121, https://doi.org/10.1007/s11069-015-2074-2.